

Utrecht University Repository

Title	Observation of the $\Omega(2012)$ baryon at the LHC
Authors	ALICE Collaboration
Published in	Physical Review D
Publication Date	2025-11-07
Link	https://dspace.library.uu.nl/handle/1874/480303
Citation	ALICE Collaboration 2025, 'Observation of the $\Omega(2012)$ baryon at the LHC', Physical Review D, vol. 112, no. 9, 092002. https://doi.org/10.1103/v4mh-3r8z
Versions / License	Publisher version
Rights	https://www.uu.nl/en/university-library/license-and-reuse-conditions

Observation of the $\Omega(2012)$ baryon at the LHC

S. Acharya *et al.**
(ALICE Collaboration)

 (Received 10 March 2025; accepted 9 September 2025; published 7 November 2025)

A signal consistent with the $\Omega(2012)$ baryon has been observed with a significance of 15σ in pp collisions at $\sqrt{s} = 13$ TeV at the LHC. In this paper, the analysis technique is described and measurements of the mass and width of the $\Omega(2012)$ are reported, along with the first measurement of its transverse-momentum spectrum and yield. This paper corroborates the observation by the Belle Collaboration of this excited Ω state and the observation that the $\Omega(2012)$ has a rather narrow width for a strongly decaying resonance. The yield measurement is combined with a statistical thermal model calculation of strange baryon yield ratios to obtain estimates of the $\Omega(2012)^- \rightarrow \Xi\bar{K}$ branching ratios. These results will improve our understanding of the internal structure and mass spectrum of excited baryon states and serve as a baseline for searches regarding modifications of these properties in high-temperature media.

DOI: [10.1103/v4mh-3r8z](https://doi.org/10.1103/v4mh-3r8z)

I. INTRODUCTION

In 2018, the Belle Collaboration reported the first observation of an excited Ω baryon state, the $\Omega(2012)$, with a significance of 7.2σ [1]. Belle discovered the particle via the decay channels $\Omega(2012)^- \rightarrow \Xi^0 K^-$, $\Omega(2012)^- \rightarrow \Xi^- K_S^0$, and their charge conjugates. The particle was reported to have a mass of $[2012.4 \pm 0.7$ (stat) ± 0.6 (sys)] MeV/ c^2 and a width of $[6.4_{-2.0}^{+2.5}$ (stat) ± 1.6 (sys)] MeV/ c^2 . In a later study, Belle reported a mass of $[2012.5 \pm 0.7$ (stat) ± 0.5 (sys)] MeV/ c^2 [2]. Belle concluded that the $\Omega(2012)^-$ is most likely to have a spin-parity configuration of $J^P = \frac{3}{2}^-$. This was partly based on theoretical studies of excited Ω baryon states [3–8]. Also, the measured width of about 6 MeV favors a d -wave decay of a $J = \frac{3}{2}$ state, rather than a significantly broader s -wave decay of a $J = \frac{1}{2}$ state. Subsequently, multiple theoretical studies have supported a $J^P = \frac{3}{2}^-$ configuration [9–20].

Measurements of such excited hadronic states provide a wealth of information relevant to several topics of interest in high-energy particle and nuclear physics. Studies of the basic properties of excited hadrons, including their masses, widths, quantum numbers, and decay branching ratios, provide important tests and inputs for theoretical models of hadron structure. Prior to the discovery of the $\Omega(2012)$, predictions of excited Ω states were obtained using various

theoretical approaches, including lattice gauge theory [3,21], the quark model [4–7,22–26], and the Skyrme model [8]. Following the discovery, multiple theoretical studies have been published that explore possible explanations of the structure of the $\Omega(2012)$ [9–19,27–35]. Some studies support the conclusion that the $\Omega(2012)$ is a regular baryon [9–16,27,28], possibly a P -wave excitation. Several works note that the mass of the $\Omega(2012)$ is just below the combined mass of the kaon and the $\Xi(1530)$ and explore the possibility that the $\Omega(2012)$ has a hadronic molecule component [17–19,29–35]. Configurations explored in these studies include $\bar{K}\Xi(1530)$ and couplings of that state to other states such as $\bar{K}\Xi$, $\Omega\eta$, and the three-quark configuration. The molecular interpretation is consistent with the recent Belle measurement of the resonant three-body decay $\Omega(2012)^- \rightarrow \Xi(1530)\bar{K} \rightarrow \Xi\pi\bar{K}$ [2].

A full understanding of the hadron chemistry of the matter produced in hadronic or nuclear collisions requires measurements of the abundances of common hadrons as well as rare, excited hadrons. To have an accurate description of hadron yields, it is necessary to understand the spectrum of excited hadronic states that decay (feed down) into lower-mass states. This includes measurements of the yields of the excited states as well as their decay modes and branching ratios into lower-mass hadrons. Complete and up-to-date lists of hadronic states are needed for implementations of the hadron resonance gas model in the framework of statistical thermal models [36–39], as well as for hadronic transport models [40–42] and hydrodynamical simulations [43,44]. Better agreement with experimental results and lattice QCD is achieved by calculations that use hadron lists with all states catalogued by the Particle Data Group (PDG), as opposed to lists that are restricted to well-established hadrons [45–47]. On the other

*Full author list given at the end of the article.

Published by the American Physical Society under the terms of the [Creative Commons Attribution 4.0 International license](https://creativecommons.org/licenses/by/4.0/). Further distribution of this work must maintain attribution to the author(s) and the published article's title, journal citation, and DOI. Funded by SCOAP³.

hand, simple quark models often overestimate the number of excited states [4,48]. Thus, experimental confirmation of rare strange resonant states such as the $\Omega(2012)$ is crucial. Accurate measurements of the properties of this state will help to improve the understanding of the spectra of excited strange baryonic states that should be included in such calculations. Furthermore, measurements of the yields of excited Ω states in nucleus-nucleus, proton-nucleus, or high-multiplicity proton-proton collisions could provide another way to explore the details of strangeness enhancement, the increase in strangeness production with increasing system size or event activity [49–54]. In addition, central heavy-ion collisions appear to produce a hadron gas phase with a lifetime of several fm/c [55,56], during which rescattering and regeneration processes can modify the yields of short-lived hadronic resonances [57–60]. Studies of how $\Omega(2012)$ yields evolve relative to the yields of the ground-state Ω could provide a new observable to improve our knowledge of the interactions in the hadronic phase and its lifetime. The number of $\Omega(2012)$ candidates found for this analysis does not allow further subdivision of the measured sample into multiplicity classes. The ongoing runs at the LHC promise to increase the available data sample by a factor of at least 50 [61]. In the future, this may enable a multiplicity-dependent study of $\Omega(2012)$ production in pp collisions, as well as measurements in p–Pb and Pb–Pb collisions, allowing the $\Omega(2012)$ to be used in hadron chemistry studies.

Furthermore, recent lattice QCD calculations of baryonic resonance properties near the pseudocritical temperature indicate that chiral symmetry restoration in the quark-gluon plasma might be verifiable through medium modification of the mass and width of parity partners [62,63]. In particular, it was shown in Ref. [64] that although the mass of the positive-parity partner stays unchanged in the crossover region, the mass of the heavier negative-parity partner is modified towards the on-shell mass of the positive-parity partner. The negative-parity baryonic states can be difficult to measure, but if the $\Omega(2012)$ is indeed the $J^P = \frac{3}{2}^-$ partner of the $\frac{3}{2}^+$ ground-state Ω , the postulated mass shift might be measurable for the $\Omega(2012)$. Since chiral symmetry restoration can manifest itself either in a mass shift or a width broadening [65,66], the requirement in both cases is to measure mass and width across a wide range of system sizes, centralities, or final-state particle multiplicities. The first mass and width measurements of the $\Omega(2012)$ [1] are for particles produced in $e^-e^+ \rightarrow \Upsilon$ annihilation events, a low-multiplicity environment. This paper presents measurements of the $\Omega(2012)$ mass and width in pp collisions with a high-multiplicity (HM) trigger. The mean charged-particle multiplicity at mid-rapidity for this data set is approximately six times larger than for inelastic pp collisions at the same energy [67]. However, far higher multiplicity values (hundreds of times larger than in inelastic pp collisions) can be reached in

nucleus-nucleus collisions [68], which produce larger and longer-lived volumes of matter in which the signatures of chiral symmetry restoration might be observed. The upgraded performance of the ALICE detector, mentioned above, may therefore also enable searches for mass and width modifications of the $\Omega(2012)$ in large collision systems.

A signal consistent with the $\Omega(2012)$ baryon has been observed by the ALICE Collaboration at the LHC. This paper describes the measurement of the $\Omega(2012)^- \rightarrow \Xi^- K_S^0$ decay and its charge conjugate in pp collisions at $\sqrt{s} = 13$ TeV. Approximately 7200 candidates are observed. Results reported here include measurements of the mass and width of the $\Omega(2012)$ and the significance of the measured signal. The first measurement of the transverse-momentum (p_T) spectrum and p_T -integrated yield of the $\Omega(2012)$ are also reported. Finally, the measured yields are used along with a statistical model calculation to estimate the branching ratios of the $\Omega(2012)^- \rightarrow \Xi \bar{K}$ decay channels. In the discussion that follows, the symbols Ω and $\bar{\Omega}(2012)$ (i.e., without superscripts indicating charges or a bar to denote antibaryons) refer to the sums of particles and antiparticles. The symbol Ω without any mass indicates the weakly decaying ground-state Ω baryon with a mass around 1672 MeV/ c^2 [69].

II. ANALYSIS PROCEDURE

A. Apparatus

A full description of the ALICE detector is provided in Refs. [70,71]. The subdetectors that are relevant to this study of the $\Omega(2012)$ are the V0 detectors [72], the Inner Tracking System (ITS) [73], the Time Projection Chamber (TPC) [74], and the Time-of-Flight (TOF) detector [75]. The V0 detectors, which provide triggering, are scintillator arrays that are located on either side of the center of the ALICE detector near the beamline; the V0A array covers the pseudorapidity range $2.8 < \eta < 5.1$, and the V0C array covers $-3.7 < \eta < -1.7$. During the data-taking period for this study, the ITS consisted of six cylindrical layers of silicon detectors that were located between 3.9 and 43 cm from the beamline. The two innermost layers of the ITS are called the Silicon Pixel Detector (SPD). The TPC is a large-volume gas detector that encloses the region with a radius from about 85 to 250 cm from the beamline. Together, the TPC and ITS span the pseudorapidity range $|\eta| < 0.9$. The ITS and TPC are used for the reconstruction of charged-particle trajectories and finding the primary collision vertex (PV). The SPD plays a role in rejecting pileup events. In addition, the TPC is used for particle identification via measurements of the specific energy loss dE/dx in the TPC gas. The TOF is a cylindrical array of multigap resistive plate chambers located beyond the outer wall of the TPC. For this study, the TOF is used in the rejection of pileup, as discussed below.

B. Dataset

The $\Omega(2012)$ baryons are reconstructed in a set of HM-triggered pp collisions at $\sqrt{s} = 13$ TeV that were recorded over 2016–2018, during Run 2 of the LHC. The trigger for inelastic pp collisions requires a coincidence of signals in the V0A and the V0C arrays. The HM trigger selects collisions which produced large signals in the V0 detectors, preferentially recording events with the highest charged-particle multiplicities, representing approximately 0%–0.1% of the visible cross section. The $\Omega(2012)$ signal is extracted from 1.04×10^9 HM-triggered events, representing an integrated luminosity of 36.6 ± 2.0 pb $^{-1}$ [76,77]. This data set has a mean charged-particle multiplicity density at midrapidity of $\langle dN_{\text{ch}}/d\eta \rangle = 31.53 \pm 0.28$ [78].

Protons circulate around the LHC in groups called “bunches.” Pileup may arise both from multiple collisions in the same bunch crossing (“in-bunch pileup”) or from collisions in other bunch crossings that did not fire the trigger, but are still within the readout time interval for some components of the ALICE detector (“out-of-bunch pileup”). The procedure for removing background and pileup collisions is adopted from Ref. [79]. Beam-induced background events are removed through use of timing information in the V0 detectors, and a selection on the correlation between clusters and tracklets in the SPD; see Ref. [71] for a detailed discussion. In-bunch pileup is removed by discarding events with multiple PVs reconstructed in the SPD. Out-of-bunch pileup events are removed through selection on multiplicity correlations in detectors that have different readout windows. Residual contributions to the $\Omega(2012)$ signal from out-of-bunch pileup are removed by requiring that at least one of the five decay product tracks of each $\Omega(2012)$ candidate is matched to a signal in the ITS or the TOF. This takes advantage of the short time resolutions for those detectors in comparison to the TPC, ensuring that the $\Omega(2012)$ candidates come from events that fired the trigger.

C. Decay reconstruction

The $\Omega(2012)$ baryon is reconstructed via the $\Omega(2012)^- \rightarrow \Xi^- K_S^0$ decay channel and its charge conjugate. The decay products are reconstructed via the decays $\Xi^- \rightarrow \pi^- \Lambda \rightarrow \pi^- (p\pi^-)$, $\bar{\Xi}^+ \rightarrow \pi^+ \bar{\Lambda} \rightarrow \pi^+ (\bar{p}\pi^+)$, and $K_S^0 \rightarrow \pi^+ \pi^-$ using the topological reconstruction techniques described in Ref. [79]. The decay product tracks are required to pass the selection criteria in the first section of Table I to ensure good track reconstruction quality and that tracks do not originate from the PV. These include selections on the track pseudorapidity, the number and fraction of readout pad rows in the ALICE TPC that were used to reconstruct the track, and the distance of closest approach (DCA) of the track to the PV. The final-state π^\pm and (anti)protons are identified via measurements in the

TABLE I. Criteria used to select V^0 and Ξ candidates. DCA stands for distance of closest approach and PV denotes the primary collision vertex. The selection criteria for $\Lambda/\bar{\Lambda}$ are given in parentheses if different from the K_S^0 selection criteria.

Decay product track selection	Selection criterion
Pseudorapidity	$ \eta < 0.8$
Number of crossed rows in TPC	≥ 70
$N_{\text{crossed}}/N_{\text{findable}}$	≥ 0.8
DCA to PV	> 0.06 cm
Pions: $(dE/dx)_{\text{TPC}} - (dE/dx)_{\text{expected}}$	$< 5\sigma_{\text{TPC}}$
p/\bar{p} : $(dE/dx)_{\text{TPC}} - (dE/dx)_{\text{expected}}$	$< 3\sigma_{\text{TPC}}$
V^0 selection	K_S^0 ($\Lambda/\bar{\Lambda}$) selection criterion
Pseudorapidity	$ \eta < 0.8$ (no selection)
Transverse decay radius	> 0.9 cm
Proper lifetime (mcL/p)	< 20 cm (< 40 cm)
DCA between decay products	< 1 (< 1.6) cm
DCA to PV	< 0.3 cm (> 0.07 cm)
Cosine of pointing angle	> 0.97
Mass tolerance	< 30 MeV/ c^2 (< 6 MeV/ c^2)
Competing V^0 rejection	< 4 MeV/ c^2 (no selection)
Ξ selection	Selection criterion
Pseudorapidity	$ \eta < 0.8$
Transverse decay radius	$0.5 < r < 100$ cm
DCA between π and Λ	< 1.4 cm
Cosine of pointing angle	> 0.97
Mass tolerance	< 7 MeV/ c^2

TPC of their specific energy loss dE/dx . It is required that π^\pm have a dE/dx within $5\sigma_{\text{TPC}}$ of the expected value, while (anti)protons must have a dE/dx within $3\sigma_{\text{TPC}}$ of the expected value, where σ_{TPC} is the TPC dE/dx resolution. The expected dE/dx values for each particle species are calculated from the Bethe-Bloch formula.

Using these π^\pm and (anti)proton tracks, displaced decay vertices are reconstructed and K_S^0 and Ξ candidates are identified by their decay topologies. K_S^0 , Λ , and $\bar{\Lambda}$ are reconstructed based on their “ V^0 ” decay topology: two oppositely charged tracks originating from the same secondary vertex, which is displaced from the PV. Ξ^- ($\bar{\Xi}^+$) are reconstructed based on their “cascade” decay topology: a Λ ($\bar{\Lambda}$) and a π^- (π^+) originating from a single decay vertex, displaced from the PV. Selections based on the decay topology are applied to improve the purity of the Ξ and K_S^0 candidates, and reduce contributions from random combinations of decay products (see Table I and discussions in Refs. [79,80]). These include selections on the DCA between the trajectories of various particles in the decay chain, the DCA between particle trajectories and the PV, the radial position of the displaced decay vertex, the particle lifetime (computed from the momentum, distance traveled, and mass hypothesis), and the difference between the

TABLE II. Contributions to the systematic uncertainties (in percent) of the results of this study. $(dN/dy)_{\text{measured}}$ refers to the p_T -integrated $\Omega(2012)$ yield over the measured region $2.2 < p_T < 10$ GeV/ c only, without p_T extrapolation. The total systematic uncertainty is the sum in quadrature of the uncertainties from the separate sources. For $d^2N/(dp_T dy)$, the percent uncertainties for the four measured p_T intervals are averaged to obtain the quoted values for each source. An empty cell indicates that an uncertainty does not apply to a given result. Negl. indicates that the contribution is negligible.

Source	Mass	Width	$d^2N/(dp_T dy)$	$(dN/dy)_{\text{measured}}$	dN/dy	$\langle p_T \rangle$
Decay product selection	0.012	13.6	6.9	3.8	3.5	0.4
Combinatorial background	Negl.	Negl.	3.4	1.5	0.7	0.5
Signal extraction	0.003	30.0	9.3	5.3	3.0	0.2
Mass shift	0.005					
Material budget			2.1	3.0	2.9	0.1
Hadronic int. cross section			0.1	0.2	0.1	Negl.
Acceptance \times efficiency			4.0	4.0	4.0	Negl.
Spectrum fit variations			1.7	0.7	+36.1 -11.5	+6.3 -12.0
Correlated between p_T intervals			5.1			
Total	0.013	32.9	13.5	8.7	+36.7 -13.4	+6.3 -12.0

measured invariant mass and the expected mass value from the PDG [69]. Selections are also applied on the cosine of the ‘‘pointing angle,’’ the angle between the momentum vector of the particle and its displacement vector (the vector connecting its production and decay points). Selection of K_S^0 candidates also employs ‘‘competing V^0 rejection:’’ the mass hypothesis for either K_S^0 decay product is changed from pion to (anti)proton; if this results in a V^0 mass within 4 MeV/ c^2 of the Λ mass, the V^0 is rejected as a K_S^0 candidate. The aforementioned selection criteria were varied during the evaluation of the systematic uncertainties; their contribution to the systematic uncertainties is listed as ‘‘decay product selection’’ in Table II. That table also lists the other systematic uncertainties which will be described in the following discussion. For each observable, the total systematic uncertainty is the sum in quadrature of the sources listed in Table II.

Each Ξ candidate is then paired with each K_S^0 candidate to obtain an invariant-mass distribution for ΞK_S^0 pairs. The Ξ and K_S^0 are assigned their respective average mass values from the PDG [69]. Each pair is required to have a rapidity within the range $|y| < 0.8$. Figure 1(a) shows the ΞK_S^0 invariant-mass distributions used for the mass and width measurements; the signal-to-background ratio is 0.033. Monte Carlo simulations indicate that the product of the acceptance and efficiency for the $\Omega(2012)$ decreases with decreasing p_T and falls below 1% for $p_T < 2$ GeV/ c (see Fig. 2 and the discussion below). The $\Omega(2012)$ yield is measured in four p_T intervals covering the range $2.2 < p_T < 10$ GeV/ c , with the low- p_T region excluded due to the lack of a significant signal. For the measurements of the mass and width of the $\Omega(2012)$, the transverse momentum is taken to be $2.5 < p_T < 10$ GeV/ c ; the larger minimum p_T value for the mass/width study is chosen to obtain a larger signal-to-background ratio. The number of ΞK_S^0 pairs that satisfy all selection criteria and

have an invariant mass $M_{\Xi K}$ in the range $2.00 < M_{\Xi K} < 2.03$ GeV/ c^2 is small compared to the number of collisions: on average, $\sim 2 \times 10^{-4}$ such $\Omega(2012)$ candidates are reconstructed per event. It is unlikely that a single event will have more than one reconstructed $\Omega(2012)$ candidate. However, if multiple candidates are identified in an event, all are kept and contribute to the invariant-mass distribution.

Two complementary methods are used to describe the background distribution. First, the event-mixing technique is employed. Each K_S^0 candidate is paired with Ξ candidates from 10 other events from the same data sample. For each pair of events that are mixed, the positions of the PVs along the beam axis are required to differ by less than 1 cm. The mixed-event background is scaled so that its integral is equal to the integral of the same-event distribution in the invariant-mass range $2.10 < M_{\Xi K} < 2.13$ GeV/ c^2 . The normalization region is varied during the evaluation of systematic uncertainties. As can be seen in Fig. 1(a), this mixed-event background can roughly describe the shape of the combinatorial background, but a residual background remains. This background includes contributions from jets, decays of other particles in which one or more products are misidentified or missed, and uncorrelated combinations of particles that mimic the V^0 or cascade topology. The mixed-event background distribution is subtracted from the same-event distribution and the result is fitted. The fit function consists of a function that describes the peak (described below), added to a second-order polynomial, which parametrizes the residual background.

In the second method used to describe the combinatorial background, the same-event invariant-mass distribution is fitted directly (without subtracting the mixed-event background). The fit function consists of a function that describes the peak (described below), added to a background function of the form

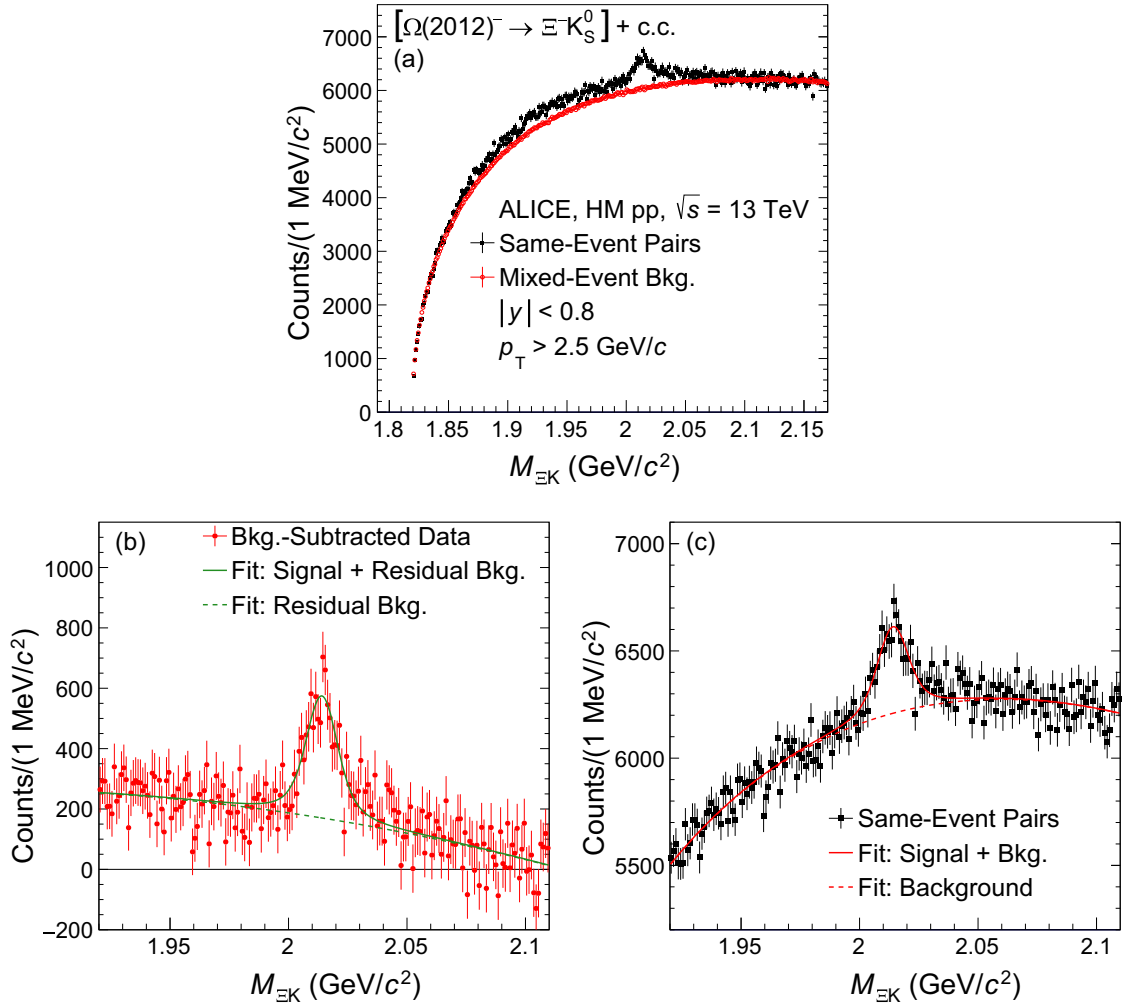


FIG. 1. Invariant-mass distributions of ΞK_S^0 pairs with $p_T > 2.5$ GeV/c and $|y| < 0.8$ in HM-triggered pp collisions at $\sqrt{s} = 13$ TeV. (a) Same-event distribution plotted with normalized mixed-event combinatorial background. (b) Background-subtracted distribution fitted with residual background polynomial and Voigt peak. (c) Same-event distribution fitted with summed background function and Voigt peak.

$$B(M_{\Xi K}) = b_0 + b_1 M_{\Xi K} + b_2 M_{\Xi K}^2 + b_3 \sqrt{M_{\Xi K} - M_{\Xi} - M_K}, \quad (1)$$

where b_0 , b_1 , b_2 , and b_3 are free parameters. M_{Ξ} and M_K are the average mass values of the Ξ^- and K^0 from the PDG [69]. The addition of the square-root term assists in describing the greater curvature on the low-mass side of the $\Omega(2012)$ peak; a similar term was used in the Φ -meson studies described in Refs. [81,82] for the same reason. The fitting procedure for these two methods is illustrated in Figs. 1(b) and 1(c). The results obtained using the two methods are compatible within several percent. They are compared during the calculation of the systematic uncertainties (listed as “combinatorial background” in Table II), and their arithmetic mean is used to calculate the mass, width, and yield values.

In all cases, a Voigt function is used to parametrize the signal component. This function has the form given in

Eq. (2) below. It is the convolution of a Breit-Wigner distribution and a Gaussian (which describes the mass resolution), as follows:

$$P(M_{\Xi K}) = \frac{A\Gamma}{(2\pi)^{3/2}\sigma} \int_{-\infty}^{\infty} \exp\left[-\frac{(M_{\Xi K} - m')^2}{2\sigma^2}\right] \times \frac{1}{(m' - \mu)^2 + \Gamma^2/4} dm'. \quad (2)$$

Here, A is a scale factor, Γ is the Breit-Wigner width parameter, σ is the Gaussian resolution parameter, μ is the most probable value of the distribution, and m' is the variable of integration. Monte Carlo simulations (described below) indicate that the σ parameter of the Voigt peak is approximately 6 MeV/c², increasing with the transverse momentum of the decaying $\Omega(2012)$. This is of the same order of magnitude as the width Γ of the resonance, which

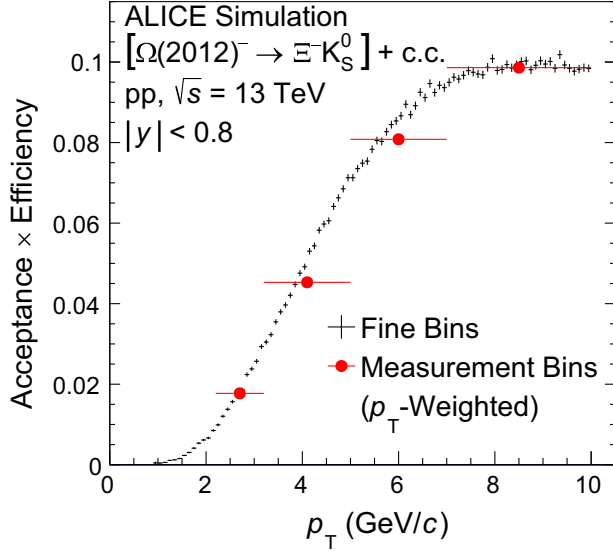


FIG. 2. Product of the acceptance and efficiency ($A \times \epsilon$) for $\Omega(2012)$ baryons within the rapidity range $|y| < 0.8$ in pp collisions at $\sqrt{s} = 13$ TeV. The value of $A \times \epsilon$ is shown in the same wide p_T bins as used in the measurement of the p_T spectrum in the real data (after the p_T -weighting procedure) and also in fine p_T bins. Only statistical uncertainties are shown.

motivates the choice of the Voigt function to describe the peak. The resolution parameter σ is fixed to the value extracted from the aforementioned simulations for each p_T bin. In the evaluation of the systematic uncertainties, σ is fixed to the lowest and highest simulation values (described below), and alternatively, the Breit-Wigner width parameter Γ of the Voigt peak is fixed to the Belle value [1]. The invariant-mass distribution is fitted over the range $1.92 < M_{\Xi K} < 2.11$ GeV/ c^2 , with several alternate intervals used during the evaluation of the systematic uncertainties. The mass and width are extracted from these fits. The simulations indicate that, due to detector effects in the $\Omega(2012)$ reconstruction procedure, the reconstructed $\Omega(2012)$ mass is 0.48 ± 0.11 MeV/ c^2 larger than the generated (initial) mass. The measured $\Omega(2012)$ mass is corrected to account for this, and the associated uncertainty is listed as “mass shift” in Table II.

The yield is calculated by subtracting the integral of the background function from integral of the same-event invariant-mass distribution over the range $2.00 < M_{\Xi K} < 2.03$ GeV/ c^2 . The yield outside this integration range is computed by integrating the tails of the peak fit function. This accounts for about 15% of the peak area and is added to the yield as a correction. Alternatively, the yield can be extracted directly from the fit function, but the resulting variations in the yields are well within the systematic uncertainties. The systematic uncertainty due to variations in how the Voigt function σ and Γ parameters are fixed, fitting range, and invariant-mass bin width is listed as “signal extraction” in Table II.

D. Parametrized spectrum

Several components of this analysis (discussed in subsequent sections) require a realistic estimate of the shape of the $\Omega(2012)p_T$ spectrum for HM pp collisions at $\sqrt{s} = 13$ TeV. In particular, the spectral shape is needed to properly weight the calculations of the acceptance and efficiency, mass resolution, and mean mass shift. A realistic p_T spectral shape is also needed to extrapolate the $\Omega(2012)$ yield to the unmeasured p_T region. However, since this paper reports the first measurement of the $\Omega(2012)p_T$ spectrum, an independent estimate of the spectral shape is needed.

To derive such a spectrum, the following procedure is used. First, the measured Ωp_T spectra in pp collisions at $\sqrt{s} = 13$ TeV [79] in different charged-particle multiplicity classes are fitted with a Lévy-Tsallis function [83–85], as follows:

$$\frac{d^2N}{dp_T dy} = p_T \times \frac{A(n-1)(n-2)}{nC[nC + M(n-2)]} \left[1 + \frac{\sqrt{p_T^2 + M^2} - M}{nC} \right]^{-n}. \quad (3)$$

Here, A , C , and n are free parameters, while M is fixed to the Ω mass. The parameters C and n are observed to increase approximately linearly with increasing $\langle dN_{ch}/d\eta \rangle$, the mean charged-particle multiplicity density at midrapidity. Next, linear functions are used to extrapolate the parameters C and n to $\langle dN_{ch}/d\eta \rangle = 31.53$, the mean multiplicity for the data sample in which this $\Omega(2012)$ study is performed [78]. Then an m_T -scaling procedure is used to convert the ground-state Ωp_T spectrum to an estimated p_T spectrum for the $\Omega(2012)$. The m_T -scaling hypothesis assumes that the invariant cross section

$$E \frac{d^3\sigma}{d^3p} = \frac{d^3\sigma}{d\phi dy p_T dp_T} = \frac{d^3\sigma}{d\phi dy m_T dm_T}$$

has the same shape as a function of $m_T \equiv \sqrt{p_T^2 + M^2}$ for all baryons. In Refs. [81,85], baryon spectra measured at STAR and ALICE in inelastic pp collisions appear to follow common trends as functions of m_T , consistent with this hypothesis. The $\Omega(2012)p_T$ spectrum is taken to have the same form as Eq. (3) with the substitution $\sqrt{p_T^2 + M^2} \rightarrow \sqrt{p_T^2 + M_{\Omega(2012)}^2}$. The remaining instances of the mass parameter M are fixed to the ground-state Ω mass, and the parameters C and n are fixed to the values derived from the ground-state Ωp_T spectra as discussed above. It has been verified that the ground-state Ωp_T spectrum in the highest measured multiplicity class in pp collisions at $\sqrt{s} = 13$ TeV can be reproduced within its uncertainties through a similar m_T -scaling procedure, starting from the $\Xi^- p_T$ spectrum. The parametrized $\Omega(2012)$ spectrum is shown in Fig. 4, along with the

measured p_T spectrum (discussed below). Alternate parametrized p_T spectra are obtained through m_T scaling of other baryon p_T spectra, using an m_T -scaled Ω spectrum without multiplicity extrapolation, and extrapolating the Lévy-Tsallis parameters to a larger multiplicity value, $\langle dN_{\text{ch}}/d\eta \rangle = 35.82$ (corresponding approximately to the 0–0.01% of the visible cross section with the highest multiplicities) [78]. The results of this study are found to be largely insensitive to the choice of the p_T spectral shape. As discussed below, the alternate p_T spectra are used to calculate systematic uncertainties for the affected observables.

E. Quantities derived from simulations

To evaluate the resolution parameter of the Voigt function, the mass shift, and the product of the acceptance and reconstruction efficiency for the $\Omega(2012)$, simulations of $\Omega(2012)$ baryons embedded into PYTHIA 8 [86,87] events were produced. The masses of the embedded $\Omega(2012)$ baryons followed a Breit-Wigner distribution with the width and most probable value set to the values measured by Belle [1]. The simulated final-state particles were propagated through a GEANT 4 [88] simulation of the ALICE detector and the same reconstruction procedures that were used for the real data.

The product of the acceptance and the efficiency, denoted $A \times \epsilon$, is the fraction of the $\Omega(2012)$ originally generated in the simulation that go on to be successfully reconstructed, with all decay products satisfying the selection criteria. This quantity is shown in Fig. 2 as a function of p_T for the rapidity range $|y| < 0.8$. It is observed that $A \times \epsilon$ for the $\Omega(2012)$ is independent of the particle’s mass, allowing for the use of an unmodified Voigt function to describe the peak. The $\Omega(2012)$ yield in each p_T interval is corrected by $A \times \epsilon$ to obtain the p_T spectrum shown in Fig. 4. In order to account for possible multiplicity mismatches between the real data and the simulation, a constant 4% systematic uncertainty is assumed to be associated with $A \times \epsilon$, contributing to the systematic uncertainties for the p_T -differential and p_T -integrated $\Omega(2012)$ yields. This value is derived from Refs. [79,89,90], in which a constant 2% systematic uncertainty is applied to K_S^0 , Λ , Ξ , and Ω yield measurements in pp and p–Pb collisions to account for possible multiplicity dependence of the efficiencies. The $\Omega(2012)$ decays to a K_S^0 and a Ξ , so the linear sum of the two $A \times \epsilon$ uncertainties for those decay products is assumed for this study. This uncertainty is listed as “acceptance \times efficiency” in Table II. The statistical uncertainty of $A \times \epsilon$ is negligible for the four wide p_T bins in which the yield is measured. The simulated $\Omega(2012)$ were uniformly distributed in transverse momentum over the range $1 < p_T < 10$ GeV/ c . Therefore, during the $A \times \epsilon$ calculation, the simulated $\Omega(2012)$ are weighted based on their p_T , using the parametrized p_T spectrum described in Sec. II D. The $A \times \epsilon$, and therefore the $\Omega(2012)$ yield, has only a small

dependence on the parametrized p_T spectrum. The “spectrum fit variations” systematic uncertainty listed in Table II is estimated from the variations in the p_T -differential $\Omega(2012)$ yield when alternate parametrized p_T spectra are used to calculate $A \times \epsilon$.

The mass resolution and mean mass shift (average difference between the generated and reconstructed masses) are also extracted from these simulations. The resolution is used in the Voigt fits described above, while the mass shift is used to correct the measured mass. Multiple techniques are used to extract these quantities, which are used to obtain their systematic uncertainties. First, the reconstructed mass distribution is fitted with a Voigt function. Second, the difference $\Delta M \equiv M_{\text{reconstructed}} - M_{\text{generated}}$ is calculated for each simulated $\Omega(2012)$, and the resolution and mean mass shift are extracted from the ΔM distribution. The extracted parameters are weighted to account for the expected p_T distribution for reconstructed $\Omega(2012)$ baryons, which is the product of the parametrized p_T spectrum, the acceptance, and the efficiency (more details on these factors are presented below). The systematic uncertainties of the resolution and mass shift also account for the use of alternate parametrized p_T spectra in this weighting procedure.

III. RESULTS

A. Mass and width

The mass and width of the $\Omega(2012)$ are observed to be

$$M_{\Omega(2012)} = [2013.35 \pm 0.57(\text{stat}) \pm 0.27(\text{sys})] \text{ MeV}/c^2, \quad (4)$$

$$\Gamma_{\Omega(2012)} = [6.2 \pm 2.1(\text{stat}) \pm 2.0(\text{sys})] \text{ MeV}/c^2. \quad (5)$$

Figure 3 shows comparisons of these values to the measurements by Belle [1,2]. The ALICE mass value has smaller uncertainties than the Belle measurements and is consistent with both of them. The ALICE measurement of the $\Omega(2012)$ width is consistent with the Belle measurement and the two have similar uncertainties.

The significance of the observed $\Omega(2012)$ signal for $p_T > 2.5$ GeV/ c is 15σ . This is evaluated as $S/\sqrt{S+B}$, where S is the number of signal counts measured in the range $2.00 < M_{\Xi K} < 2.03$ GeV/ c^2 and $S+B$ is the combined number of signal and background counts in the same range (without subtraction of the mixed-event background). The first observation of the $\Omega(2012)$, reported by the Belle Collaboration [1], had a significance of 7.2σ .

B. Yields

The $\Omega(2012)$ transverse-momentum spectrum, not corrected for the unmeasured $\Omega(2012) \rightarrow \Xi K_S^0$ branching ratio, is shown in Fig. 4. Small additional systematic

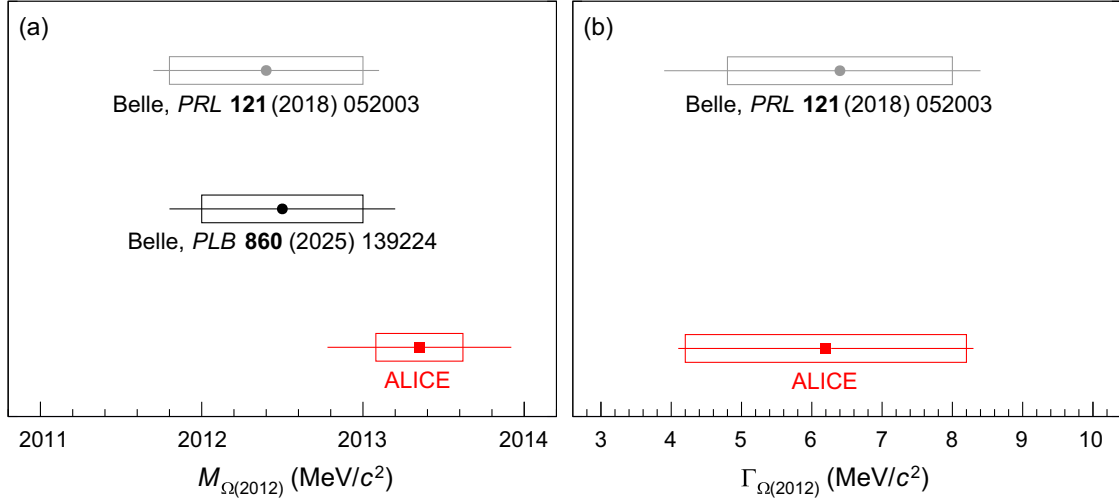


FIG. 3. Comparison of mass (a) and width (b) measurements of the $\Omega(2012)$. The plotted results are from Belle [1,2] and ALICE (this work). Statistical uncertainties are shown as bars, and systematic uncertainties are shown as boxes.

uncertainties arise from imperfect knowledge of the ALICE material budget and the hadronic interaction cross sections for the decay products; these uncertainties were evaluated as in Ref. [79] and are listed in Table II. The integrated $\Omega(2012)$ yield for $2.2 < p_T < 10$ GeV/c (not corrected for the unmeasured branching ratio) is found to be

$$\begin{aligned} \mathcal{B}[\Omega(2012)^- \rightarrow \Xi^- K_S^0] \times (dN/dy)_{\text{measured}} \\ = [1.75 \pm 0.20(\text{stat}) \pm 0.15(\text{sys})] \times 10^{-4}. \end{aligned} \quad (6)$$

For the p_T spectrum, the ‘‘material budget,’’ ‘‘hadronic interaction cross section,’’ and ‘‘acceptance \times efficiency’’ systematic uncertainties are assumed to be fully correlated between p_T intervals. The ‘‘decay product selection,’’ ‘‘combinatorial background,’’ and ‘‘signal extraction’’ uncertainties may have both p_T -correlated and p_T -uncorrelated components. To determine the p_T -correlated component, the parameters of the analysis (decay product selections, combinatorial background, fit range, etc.) are varied and the resulting variations in $(dN/dy)_{\text{measured}}$ are compared to the variations of the yields in the individual p_T intervals. From this comparison, it is found that the total p_T -correlated component of these uncertainties is 2.3% of the yield; the combination of this contribution and the three fully p_T -correlated uncertainties is 5.1% on average.

The spectrum is fitted with the aforementioned parameterized p_T spectrum function, with only the overall scale factor allowed to vary. The full p_T -integrated $\Omega(2012)$ yield is the sum of the yields measured in each of the four p_T bins, added to the extrapolated yields (derived from the fit function) for the unmeasured low- and high- p_T regions. The mean transverse momentum $\langle p_T \rangle$ is calculated as follows:

$$\langle p_T \rangle = \frac{\sum_{j=0}^5 (\langle p_T \rangle_j \times Y_j)}{\sum_{j=0}^5 Y_j}. \quad (7)$$

In the sums, bins 1–4 are the measured p_T bins, while bins 0 and 5 are the unmeasured low- and high- p_T regions, respectively. The Y_j values are the $\Omega(2012)$ yields (dN/dy) in each bin. The yields Y_0 and Y_5 are calculated by integrating the fit function, while the other Y_j values are the measured values shown in Fig. 4 (scaled by the p_T bin width). The mean transverse momentum in each bin is denoted $\langle p_T \rangle_j$; all six values are extracted from the fit function.

Additional systematic uncertainties on these quantities are estimated by using alternate fits to extrapolate the yield; this uncertainty is listed as ‘‘spectrum fit variations’’ in Table II. The considered variations include the use of different fitting ranges, the alternate parameterized p_T spectra (obtained from measurements of other baryons as described above), m_T -exponential, Boltzmann, and Fermi-Dirac distributions, and an unconstrained Levy-Tsallis function. The full p_T -integrated $\Omega(2012)$ yield (not corrected for the unmeasured branching ratio) and the mean transverse momentum are observed to be

$$\begin{aligned} \mathcal{B}[\Omega(2012)^- \rightarrow \Xi^- K_S^0] \times dN/dy \\ = [4.2 \pm 0.3(\text{stat})_{-0.6}^{+1.5}(\text{sys})] \times 10^{-4}, \end{aligned} \quad (8)$$

$$\langle p_T \rangle = [2.15 \pm 0.08(\text{stat})_{-0.26}^{+0.14}(\text{sys})] \text{ GeV}/c. \quad (9)$$

C. Branching ratios

Experimental $\Omega(2012)$ and Ω yields can be used together with a statistical model calculation of the $\Omega(2012)/\Omega$ yield ratio to obtain an estimate of the $\Omega(2012)^- \rightarrow \Xi \bar{K}$ branching ratios. This measurement was obtained for HM pp

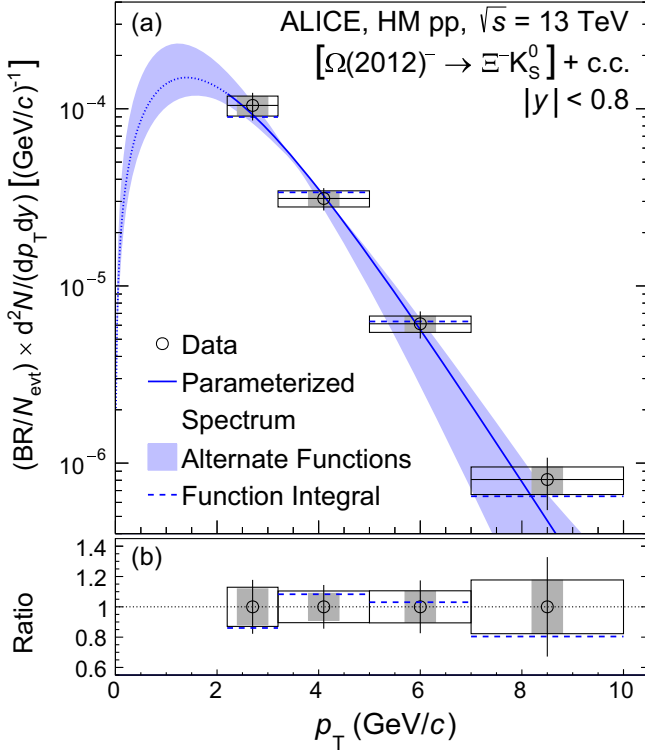


FIG. 4. (a) p_T spectrum of the $\Omega(2012)$ in HM pp collisions at $\sqrt{s} = 13$ TeV (not corrected for the unmeasured branching ratio (BR) for the studied decay channel). Vertical bars represent statistical uncertainties, empty boxes represent the total systematic uncertainties, and shaded boxes represent the portion of the systematic uncertainties that is uncorrelated between p_T intervals (only slightly smaller than the total systematic uncertainties). The data points are plotted at the center of each p_T interval and the horizontal bars and boxes span the entire width of each p_T interval. The curve is the parameterized spectrum for the $\Omega(2012)$ baryon. The shaded band surrounding the curve indicates the region spanned by the envelope of alternate functions used to describe the spectrum, which affect the extrapolation of the yield to low p_T . The horizontal dashed lines labeled “Function Integral” show the integral of the parameterized spectrum over each of the four measured p_T intervals. (b) The horizontal dashed lines show the ratio of the parameterized yield to the measured $\Omega(2012)$ yield in each of the four p_T intervals. The bars and boxes indicate the fractional uncertainties (statistical, total systematic, and p_T -uncorrelated systematic) of the measured data.

collisions, but a measurement of the corresponding ground-state Ω yield has not yet been published. Therefore, the Ω yield is estimated by interpolation of previous ALICE measurements in pp collisions at $\sqrt{s} = 13$ TeV at lower multiplicities [79] and in p–Pb collisions at $\sqrt{s_{NN}} = 5.02$ TeV [89]. The Ω yields appear to follow the same trend as a function of $\langle dN_{ch}/d\eta \rangle$, independent of collision system or energy. The interpolation is performed using a function of the form

$$dN_{\Omega}/dy = A \langle dN_{ch}/d\eta \rangle^n, \quad (10)$$

where A and n are free parameters. The interpolated Ω yield at $\langle dN_{ch}/d\eta \rangle = 31.53$ is estimated to be 0.0179 ± 0.0023 . The uncertainty of the interpolated Ω yield originates from the uncertainties of the measured yields, including statistical, multiplicity-uncorrelated systematic, and multiplicity-correlated systematic contributions.

The observed $\langle dN_{ch}/d\eta \rangle$ dependence of the Ω yields in pp and p–Pb collisions is well described by statistical thermal models formulated in the canonical ensemble with charge conservation [91–95]. In Ref. [93], analytic parametrizations were obtained to find statistical thermal model parameters as functions of $\langle dN_{ch}/d\eta \rangle$. For $\langle dN_{ch}/d\eta \rangle = 31.53$, these parametrizations give a chemical freeze-out temperature of $T = 167$ MeV, a system volume per unit rapidity of $dV/dy = 75.7$ fm³, and a strangeness suppression factor of $\gamma_S = 0.853$. Since the Ω and $\Omega(2012)$ have the same minimal quark content, their yields should evolve similarly as a function of $\langle dN_{ch}/d\eta \rangle$, and any dependence on dV/dy or γ_S will cancel. The ratio of the Ω and $\Omega(2012)$ yields should depend only on the chemical freeze-out temperature of the system, and the masses and spins of the Ω and $\Omega(2012)$. The $\Omega(2012)/\Omega$ yield ratio reduces to the thermal density ratio in the grand canonical ensemble [50], as follows:

$$\frac{\Omega(2012)_{SM}}{\Omega_{SM}} = \frac{2J_{\Omega(2012)} + 1}{2J_{\Omega} + 1} \times \frac{M_{\Omega(2012)}^2}{M_{\Omega}^2} \times \frac{K_2(M_{\Omega(2012)}/T)}{K_2(M_{\Omega}/T)}. \quad (11)$$

Here, M and J denote the masses and spins of the particles, T denotes the chemical freeze-out temperature, and K_2 is the modified Bessel function of the second type with order 2. For the sake of brevity, here and below, the particle symbols Ω and $\Omega(2012)$ are used to represent the particle yields dN_{Ω}/dy and $dN_{\Omega(2012)}/dy$. Using $T = 167$ MeV, the value for $M_{\Omega(2012)}$ reported in this paper, and $J_{\Omega(2012)} = \frac{3}{2}$, it is found that $\Omega(2012)_{SM}/\Omega_{SM} = 0.1666$. Assuming $J_{\Omega(2012)} = \frac{1}{2}$ scales the yield ratio by a factor of 0.5, while assuming $J_{\Omega(2012)} = \frac{5}{2}$ scales the yield ratio by a factor of 1.5. The following calculations assume $J_{\Omega(2012)} = \frac{3}{2}$ for the reasons discussed in the introduction. It has been verified that other thermal-model implementations reproduce the analytic result described above. Using the T , dV/dy , and γ_S values extracted from Ref. [93], the Thermal-FIST framework [96] reproduces the $\Omega(2012)/\Omega$ yield ratio found using Eq. (11). A calculation following Ref. [95] with $T = 156.5$ MeV also reproduces the analytic result. A ± 11 MeV uncertainty is assigned to the chemical freeze-out temperature. This covers the range of variation in the extracted temperature from recent thermal-model fits of light-flavor hadron yields for collision systems with $\langle dN_{ch}/d\eta \rangle \approx 30$ [91–95]. This translates into a $\pm 13\%$

uncertainty in the $\Omega(2012)/\Omega$ yield ratio. Using the mass values reported by Belle [1,2] results in a negligible change in this yield ratio.

Combining these results, an estimate of the $\Omega(2012)^- \rightarrow \Xi^- \bar{K}^0$ branching ratio is obtained:

$$\begin{aligned} \mathcal{B}[\Omega(2012)^- \rightarrow \Xi^- \bar{K}^0] &= \frac{2 \times \mathcal{B}[\Omega(2012)^- \rightarrow \Xi^- K_S^0] \times \Omega(2012)_{\text{ALICE}}}{\Omega_{\text{ALICE}}} \\ &\times \frac{\Omega_{\text{SM}}}{\Omega(2012)_{\text{SM}}} = 0.28_{-0.07}^{+0.12}. \end{aligned} \quad (12)$$

The factor of 2 accounts for the fact that only half of the produced K^0 and \bar{K}^0 mesons decay as K_S^0 . The largest contribution to the uncertainty comes from the ALICE $\Omega(2012)$ yield, with other independent contributions coming from the uncertainties in the interpolated ALICE Ω yield and the ± 10 MeV variation in the temperature, which affects the thermal-model calculation of the $\Omega(2012)/\Omega$ yield ratio.

Belle reported [1] that the ratio of the two-body branching ratios is

$$\frac{\mathcal{B}[\Omega(2012)^- \rightarrow \Xi^0 K^-]}{\mathcal{B}[\Omega(2012)^- \rightarrow \Xi^- \bar{K}^0]} = 1.2 \pm 0.3. \quad (13)$$

From this, the branching ratio for $\Omega(2012)^- \rightarrow \Xi^0 K^-$ and the combined two-body branching ratio for $\Omega(2012)^- \rightarrow \Xi \bar{K}$ are estimated, as follows:

$$\mathcal{B}[\Omega(2012)^- \rightarrow \Xi^0 K^-] = 0.34_{-0.12}^{+0.16}, \quad (14)$$

$$\mathcal{B}[\Omega(2012)^- \rightarrow \Xi \bar{K}] = 0.62_{-0.17}^{+0.27}. \quad (15)$$

The Belle Collaboration has measured the three-body $\Omega(2012) \rightarrow \Xi \pi \bar{K}$ decays [2]. It was observed that these occur predominantly through the resonant channel $\Omega(2012) \rightarrow \Xi(1530) \bar{K} \rightarrow \Xi \pi \bar{K}$, with no significant non-resonant contribution seen. It was found that the ratio of the three-body branching fraction to the two-body branching fraction is $\mathcal{R}_{\Xi \bar{K}}^{\Xi \pi \bar{K}} = 0.99 \pm 0.26 \pm 0.06$. Under the assumption that all $\Omega(2012)$ decays are either $\Omega(2012)^- \rightarrow \Xi \bar{K}$ or $\Omega(2012)^- \rightarrow \Xi \pi \bar{K}$, the Belle measurement of $\mathcal{R}_{\Xi \bar{K}}^{\Xi \pi \bar{K}}$ would imply a two-body branching ratio $\mathcal{B}[\Omega(2012)^- \rightarrow \Xi \bar{K}] = 0.50_{-0.06}^{+0.08}$; the ALICE estimate is consistent with this value within uncertainties. Thus, the measured branching ratios reported in Eqs. (12), (14), and (15), as well as the Belle measurement of $\mathcal{R}_{\Xi \bar{K}}^{\Xi \pi \bar{K}}$, disfavor models of the $\Omega(2012)$ structure that require large branching ratios (close to unity) for the three-body decays.

The preceding calculations assumed $J_{\Omega(2012)} = \frac{3}{2}$. If it is assumed $J_{\Omega(2012)} = \frac{1}{2}$, then the combined two-body branching ratio would have a lower limit of 0.9, which is incompatible with the Belle measurement of $\mathcal{R}_{\Xi \bar{K}}^{\Xi \pi \bar{K}}$. This

reinforces the arguments discussed earlier that the $\Omega(2012)$ is most likely to have a spin of $\frac{3}{2}$.

A cross-check of this branching-ratio study has been performed using measurements and model calculations of the $\Xi(1530)^0/\Xi^-$ yield ratio (where the particle symbols should be interpreted as also representing the antiparticles). In the ALICE Collaboration's measurement of $\Xi(1530)^0$ yields as a function of $\langle dN_{\text{ch}}/d\eta \rangle$ in pp collisions at $\sqrt{s} = 13$ TeV, the measured $\Xi(1530)^0$ yield was corrected for the $\Xi(1530)^0 \rightarrow \Xi^- \pi^+$ branching ratio [97]. That branching ratio was assumed to be exactly $\frac{2}{3}$, based on isospin considerations and value of the total $\Xi(1530)^0 \rightarrow \Xi \pi$ branching ratio, which is 100% [69]. Under this assumption, the $\Xi(1530)^0/\Xi^-$ yield ratio was reported to be $0.332 \pm 0.012(\text{stat.}) \pm 0.051(\text{sys.})$ for the highest multiplicity interval reported, with $\langle dN_{\text{ch}}/d\eta \rangle = 18.67 \pm 0.20$. Statistical models also assume that the $\Xi(1530)^0 \rightarrow \Xi^- \pi^+$ branching ratio is $\frac{2}{3}$, which is relevant for the calculation of the feed-down of $\Xi(1530)^0$ to Ξ^- . A calculation following Ref. [95] gives $\Xi(1530)^0/\Xi^- = 0.36$. If model parameters are extracted based on the parametrizations in Ref. [93], then used with the Thermal-FIST framework [96], the yield ratio is found to be $\Xi(1530)^0/\Xi^- = 0.38$. The model calculations of the $\Xi(1530)^0/\Xi^-$ yield ratio, the ALICE measurement of that ratio, and the branching ratio value are all consistent with each other. This indicates that model and experimental yield-ratio values can be employed to estimate unknown branching ratios for other multistrange baryons, as was done above for the $\Omega(2012)$.

IV. CONCLUSION

In summary, the study reported in this paper corroborates the discovery of the $\Omega(2012)$ baryon. A signal with a significance of 15σ has been observed in high-multiplicity-triggered pp collisions at $\sqrt{s} = 13$ TeV. The mass and width of the particle are measured to be $[2013.35 \pm 0.57(\text{stat}) \pm 0.27(\text{sys})]$ MeV/ c^2 and $[6.2 \pm 2.1(\text{stat}) \pm 2.0(\text{sys})]$ MeV/ c^2 , respectively; these values are consistent with the previous measurements by Belle [1,2]. The first measurement of the p_T -dependent and p_T -integrated production yield of the $\Omega(2012)$ baryon has also been reported, along with a measurement of its mean transverse momentum. Furthermore, based on a comparison to the statistical thermal model expectation, the total branching ratio for the $\Omega(2012)^- \rightarrow \Xi \bar{K}$ decays is estimated to be $0.62_{-0.17}^{+0.27}$. These results may provide useful information for studies of the structure of the $\Omega(2012)$ and the chemistry of the matter produced in high-energy hadronic and nuclear collisions. The LHC is in its third running period and the ALICE detector has been upgraded, significantly increasing the number of events it can record. This advancement, combined with implementation of

machine-learning techniques to identify $\Omega(2012)$ candidates, may enable further, more precise measurements of $\Omega(2012)$ production and properties and may allow for a search for the signatures of chiral symmetry restoration using excited Ω baryons.

ACKNOWLEDGMENTS

The ALICE Collaboration would like to thank all its engineers and technicians for their invaluable contributions to the construction of the experiment and the CERN accelerator teams for the outstanding performance of the LHC complex. The ALICE Collaboration gratefully acknowledges the resources and support provided by all Grid centers and the Worldwide LHC Computing Grid (WLCG) collaboration. The ALICE Collaboration acknowledges the following funding agencies for their support in building and running the ALICE detector: A. I. Alikhanyan National Science Laboratory (Yerevan Physics Institute) Foundation (ANSL), State Committee of Science and World Federation of Scientists (WFS), Armenia; Austrian Academy of Sciences, Austrian Science Fund (FWF): [M 2467-N36] and Nationalstiftung für Forschung, Technologie und Entwicklung, Austria; Ministry of Communications and High Technologies, National Nuclear Research Center, Azerbaijan; Conselho Nacional de Desenvolvimento Científico e Tecnológico (CNPq), Financiadora de Estudos e Projetos (Finep), Fundação de Amparo à Pesquisa do Estado de São Paulo (FAPESP) and Universidade Federal do Rio Grande do Sul (UFRGS), Brazil; Bulgarian Ministry of Education and Science, within the National Roadmap for Research Infrastructures 2020-2027 (object CERN), Bulgaria; Ministry of Education of China (MOEC), Ministry of Science & Technology of China (MSTC) and National Natural Science Foundation of China (NSFC), China; Ministry of Science and Education and Croatian Science Foundation, Croatia; Centro de Aplicaciones Tecnológicas y Desarrollo Nuclear (CEADEN), Cubaenergía, Cuba; Ministry of Education, Youth and Sports of the Czech Republic, Czech Republic; The Danish Council for Independent Research | Natural Sciences, the VILLUM FONDEN and Danish National Research Foundation (DNRF), Denmark; Helsinki Institute of Physics (HIP), Finland; Commissariat à l’Energie Atomique (CEA) and Institut National de Physique Nucléaire et de Physique des Particules (IN2P3) and Centre National de la Recherche Scientifique (CNRS), France; Bundesministerium für Bildung und Forschung (BMBF) and GSI Helmholtzzentrum für Schwerionenforschung GmbH, Germany; General Secretariat for Research and Technology, Ministry of Education, Research and Religions, Greece; National Research, Development and Innovation Office, Hungary; Department of Atomic Energy Government of India (DAE), Department of Science and Technology, Government of India (DST), University Grants Commission, Government of India

(UGC) and Council of Scientific and Industrial Research (CSIR), India; National Research and Innovation Agency–BRIN, Indonesia; Istituto Nazionale di Fisica Nucleare (INFN), Italy; Japanese Ministry of Education, Culture, Sports, Science and Technology (MEXT) and Japan Society for the Promotion of Science (JSPS) KAKENHI, Japan; Consejo Nacional de Ciencia (CONACYT) y Tecnología, through Fondo de Cooperación Internacional en Ciencia y Tecnología (FONCICYT) and Dirección General de Asuntos del Personal Académico (DGAPA), Mexico; Nederlandse Organisatie voor Wetenschappelijk Onderzoek (NWO), Netherlands; the Research Council of Norway, Norway; Pontificia Universidad Católica del Perú, Peru; Ministry of Science and Higher Education, National Science Centre and WUT ID-UB, Poland; Korea Institute of Science and Technology Information and National Research Foundation of Korea (NRF), Republic of Korea; Ministry of Education and Scientific Research, Institute of Atomic Physics, Ministry of Research and Innovation and Institute of Atomic Physics and Universitatea Nationala de Stiinta si Tehnologie Politehnica Bucuresti, Romania; Ministry of Education, Science, Research and Sport of the Slovak Republic, Slovakia; National Research Foundation of South Africa, South Africa; Swedish Research Council (VR) and Knut & Alice Wallenberg Foundation (KAW), Sweden; European Organization for Nuclear Research, Switzerland; Suranaree University of Technology (SUT), National Science and Technology Development Agency (NSTDA) and National Science, Research and Innovation Fund (NSRF via PMU-B B05F650021), Thailand; Turkish Energy, Nuclear and Mineral Research Agency (TENMAK), Turkey; National Academy of Sciences of Ukraine, Ukraine; Science and Technology Facilities Council (STFC), United Kingdom; National Science Foundation of the United States of America (NSF) and United States Department of Energy, Office of Nuclear Physics (DOE NP), United States of America. In addition, individual groups or members have received support from: Czech Science Foundation (Grant No. 23-07499S), Czech Republic; FORTE Project, Reg. No. CZ.02.01.01/00/22_008/0004632, Czech Republic, cofunded by the European Union, Czech Republic; European Research Council (Grant No. 950692), European Union; Academy of Finland (Center of Excellence in Quark Matter) (Grants No. 346327 and No. 346328), Finland; Deutsche Forschungs Gemeinschaft (DFG, German Research Foundation) “Neutrinos and Dark Matter in Astro- and Particle Physics” (Grant No. SFB 1258), Germany; ICSC–National Research Center for High Performance Computing, Big Data and Quantum Computing and FAIR–Future Artificial Intelligence Research, funded by the NextGenerationEU program (Italy).

DATA AVAILABILITY

The data that support the findings of this article are openly available [98].

- [1] J. Yelton *et al.* (Belle Collaboration), Observation of an excited Ω^- baryon, *Phys. Rev. Lett.* **121**, 052003 (2018).
- [2] S. Jia *et al.* (Belle Collaboration), Observation of $\Omega(2012)^- \rightarrow \Xi(1530)\bar{K}$ and measurement of the effective couplings of $\Omega(2012)^- \rightarrow \Xi(1530)\bar{K}$ and $\Xi\bar{K}$, *Phys. Lett. B* **860**, 139224 (2025).
- [3] G. P. Engel, C. B. Lang, D. Mohler, and A. Schäfer (BGR Collaboration), QCD with two light dynamical chirally improved quarks: Baryons, *Phys. Rev. D* **87**, 074504 (2013).
- [4] S. Capstick and N. Isgur, Baryons in a relativized quark model with chromodynamics, *Phys. Rev. D* **34**, 2809 (1986).
- [5] U. Löring, B. C. Metsch, and H. R. Petry, The light-baryon spectrum in a relativistic quark model with instanton-induced quark forces: The strange baryon spectrum, *Eur. Phys. J. A* **10**, 447 (2001).
- [6] M. Pervin and W. Roberts, Strangeness -2 and -3 baryons in a constituent quark model, *Phys. Rev. C* **77**, 025202 (2008).
- [7] R. N. Faustov and V. O. Galkin, Strange baryon spectroscopy in the relativistic quark model, *Phys. Rev. D* **92**, 054005 (2015).
- [8] Y. Oh, Ξ and Ω baryons in the Skyrme model, *Phys. Rev. D* **75**, 074002 (2007).
- [9] L.-Y. Xiao and X.-H. Zhong, Possible interpretation of the newly observed $\Omega(2012)$ state, *Phys. Rev. D* **98**, 034004 (2018).
- [10] T. M. Aliev, K. Azizi, Y. Sarac, and H. Sundu, Interpretation of the newly discovered $\Omega(2012)$, *Phys. Rev. D* **98**, 014031 (2018).
- [11] T. M. Aliev, K. Azizi, Y. Sarac, and H. Sundu, Nature of the $\Omega(2012)$ through its strong decays, *Eur. Phys. J. C* **78**, 894 (2018).
- [12] Z.-Y. Wang, L.-C. Gui, Q.-F. Lü, L.-Y. Xiao, and X.-H. Zhong, Newly observed $\Omega(2012)$ state and strong decays of the low-lying Ω excitations, *Phys. Rev. D* **98**, 114023 (2018).
- [13] M. V. Polyakov, H.-D. Son, B.-D. Sun, and A. Tandogan, $\Omega(2012)$ through the looking glass of flavour $SU(3)$, *Phys. Lett. B* **792**, 315 (2019).
- [14] M.-S. Liu, K.-L. Wang, Q.-F. Lü, and X.-H. Zhong, Ω baryon spectrum and their decays in a constituent quark model, *Phys. Rev. D* **101**, 016002 (2020).
- [15] A. J. Arifi, D. Suenaga, A. Hosaka, and Y. Oh, Strong decays of multistrangeness baryon resonances in the quark model, *Phys. Rev. D* **105**, 094006 (2022).
- [16] K.-L. Wang, Q.-F. Lü, J.-J. Xie, and X.-H. Zhong, Toward discovering the excited Ω baryons through nonleptonic weak decays of Ω_c , *Phys. Rev. D* **107**, 034015 (2023).
- [17] Y.-H. Lin and B.-S. Zou, Hadronic molecular assignment for the newly observed Ω^* state, *Phys. Rev. D* **98**, 056013 (2018).
- [18] Y. Huang, M.-Z. Liu, J.-X. Lu, J.-J. Xie, and L.-S. Geng, Strong decay modes $\bar{K}\Xi$ and $\bar{K}\Xi\pi$ of the $\Omega(2012)$ in the $\bar{K}\Xi(1530)$ and $\eta\Omega$ molecular scenario, *Phys. Rev. D* **98**, 076012 (2018).
- [19] J.-X. Lu, C.-H. Zeng, E. Wang, J.-J. Xie, and L.-S. Geng, Revisiting the $\Omega(2012)$ as a hadronic molecule and its strong decays, *Eur. Phys. J. C* **80**, 361 (2020).
- [20] R. J. Hudspith, M. F. M. Lutz, and D. Mohler, Precise Omega baryons from lattice QCD, arXiv:2404.02769.
- [21] CLQCD Collaboration, J. Liang, W. Sun, Y. Chen, W.-F. Qiu, M. Gong, C. Liu, Y.-B. Liu, Z. Liu, J.-P. Ma, and J.-B. Zhang, Spectrum and Bethe-Salpeter amplitudes of Ω baryons from lattice QCD, *Chin. Phys. C* **40**, 041001 (2016).
- [22] K.-T. Chao, N. Isgur, and G. Karl, Strangeness -2 and -3 baryons in a quark model with chromodynamics, *Phys. Rev. D* **23**, 155 (1981).
- [23] C. S. Kalman, P -wave baryons in a consistent quark model with hyperfine interactions, *Phys. Rev. D* **26**, 2326 (1982).
- [24] J. Liu, R. D. McKeown, and M. J. Ramsey-Musolf, Global analysis of nucleon strange form factors at low Q^2 , *Phys. Rev. C* **76**, 025202 (2007).
- [25] C. S. An, B. C. Metsch, and B. S. Zou, Mixing of the low-lying three- and five-quark Ω states with negative parity, *Phys. Rev. C* **87**, 065207 (2013).
- [26] C. S. An and B. S. Zou, Low-lying Ω states with negative parity in an extended quark model with Nambu–Jona-Lasinio interaction, *Phys. Rev. C* **89**, 055209 (2014).
- [27] X. Liu, H. Huang, J. Ping, and D. Chen, Investigating $\Omega(2012)$ as a molecular state, *Phys. Rev. C* **103**, 025202 (2021).
- [28] H.-H. Zhong, R.-H. Ni, M.-Y. Chen, X.-H. Zhong, and J.-J. Xie, Further study of $\Omega^*[1P_{3/2}^-]$ within a chiral quark model, *Chin. Phys. C* **47**, 063104 (2023).
- [29] M. P. Valderrama, $\Omega(2012)$ as a hadronic molecule, *Phys. Rev. D* **98**, 054009 (2018).
- [30] R. Pavao and E. Oset, Coupled channels dynamics in the generation of the $\Omega(2012)$ resonance, *Eur. Phys. J. C* **78**, 857 (2018).
- [31] T. Gutsche and V. E. Lyubovitskij, Strong decays of the hadronic molecule $\Omega^*(2012)$, *J. Phys. G* **48**, 025001 (2020).
- [32] Y.-H. Lin, F. Wang, and B.-S. Zou, Reanalysis of the newly observed Ω^* state in a hadronic molecule model, *Phys. Rev. D* **102**, 074025 (2020).
- [33] N. Ikeno, G. Toledo, and E. Oset, Molecular picture for the $\Omega(2012)$ revisited, *Phys. Rev. D* **101**, 094016 (2020).
- [34] N. Ikeno, W.-H. Liang, G. Toledo, and E. Oset, Interpretation of the $\Omega_c \rightarrow \pi^+\Omega(2012) \rightarrow \pi^+(\bar{K}\Xi)$ relative to $\Omega_c \rightarrow \pi^+\bar{K}\Xi$ from the $\Omega(2012)$ molecular perspective, *Phys. Rev. D* **106**, 034022 (2022).
- [35] Q.-F. Lü, H. Nagahiro, and A. Hosaka, Understanding the nature of $\Omega(2012)$ in a coupled-channel approach, *Phys. Rev. D* **107**, 014025 (2023).
- [36] R. Hagedorn, Statistical thermodynamics of strong interactions at high energies, *Nuovo Cimento, Suppl.* **3** (1965) 147–186.
- [37] R. Dashen, S.-K. Ma, and H. J. Bernstein, S -Matrix formulation of statistical mechanics, *Phys. Rev.* **187**, 345 (1969); **6**, 851(E) (1972).
- [38] A. Andronic, P. Braun-Munzinger, K. Redlich, and J. Stachel, Decoding the phase structure of QCD via particle production at high energy, *Nature (London)* **561**, 321 (2018).
- [39] F. A. Flor, G. Olinger, and R. Bellwied, Flavour and energy dependence of chemical freeze-out temperatures in relativistic heavy ion collisions from RHIC-BES to LHC energies, *Phys. Lett. B* **814**, 136098 (2021).
- [40] S. Bass, M. Belkacem *et al.*, Microscopic models for ultrarelativistic heavy ion collisions, *Prog. Part. Nucl. Phys.* **41**, 255 (1998).

- [41] H. Petersen, J. Steinheimer, G. Burau, M. Bleicher, and H. Stöcker, Fully integrated transport approach to heavy ion reactions with an intermediate hydrodynamic stage, *Phys. Rev. C* **78**, 044901 (2008).
- [42] K. Werner, Core-corona procedure and microcanonical hadronization to understand strangeness enhancement in proton-proton and heavy ion collisions in the EPOS4 framework, *Phys. Rev. C* **109**, 014910 (2024).
- [43] B. Schenke, S. Jeon, and C. Gale, Higher flow harmonics from $(3+1)$ D event-by-event viscous hydrodynamics, *Phys. Rev. C* **85**, 024901 (2012).
- [44] S. Jeon and U. Heinz, Introduction to hydrodynamics, *Int. J. Mod. Phys. E* **24**, 1530010 (2015).
- [45] P. Alba *et al.*, Constraining the hadronic spectrum through QCD thermodynamics on the lattice, *Phys. Rev. D* **96**, 034517 (2017).
- [46] P. Alba, V. M. Sarti, J. Noronha-Hostler, P. Parotto, I. Portillo-Vazquez, C. Ratti, and J. M. Stafford, Influence of hadronic resonances on the chemical freeze-out in heavy-ion collisions, *Phys. Rev. C* **101**, 054905 (2020).
- [47] J. M. Karthein, V. Koch, C. Ratti, and V. Vovchenko, Constraining the hadronic spectrum and repulsive interactions in a hadron resonance gas via fluctuations of conserved charges, *Phys. Rev. D* **104**, 094009 (2021).
- [48] D. Ebert, R. N. Faustov, and V. O. Galkin, Mass spectra and Regge trajectories of light mesons in the relativistic quark model, *Phys. Rev. D* **79**, 114029 (2009).
- [49] J. Rafelski and B. Müller, Strangeness production in the quark-gluon plasma, *Phys. Rev. Lett.* **48**, 1066 (1982); **56**, 2334(E) (1986).
- [50] S. Hamieh, K. Redlich, and A. Tounsi, Canonical description of strangeness enhancement from p-A to Pb-Pb collisions, *Phys. Lett. B* **486**, 61 (2000).
- [51] E. Andersen *et al.* (WA97 Collaboration), Strangeness enhancement at mid-rapidity in Pb-Pb collisions at 158A GeV/c, *Phys. Lett. B* **449**, 401 (1999).
- [52] J. Adams *et al.* (STAR Collaboration), Multistrange baryon production in Au-Au collisions at $\sqrt{s_{NN}} = 130$ GeV, *Phys. Rev. Lett.* **92**, 182301 (2004).
- [53] B. Abelev *et al.* (ALICE Collaboration), Multi-strange baryon production at mid-rapidity in Pb-Pb collisions at $\sqrt{s_{NN}} = 2.76$ TeV, *Phys. Lett. B* **728**, 216 (2014); **734**, 409 (E) (2014).
- [54] J. Adam *et al.* (ALICE Collaboration), Enhanced production of multi-strange hadrons in high-multiplicity proton-proton collisions, *Nat. Phys.* **13**, 535 (2017).
- [55] S. Acharya *et al.* (ALICE Collaboration), Evidence of rescattering effect in Pb-Pb collisions at the LHC through production of $K^*(892)^0$ and $\phi(1020)$ mesons, *Phys. Lett. B* **802**, 135225 (2020).
- [56] A. G. Knospe, C. Markert, K. Werner, J. Steinheimer, and M. Bleicher, Hadronic resonance production and interaction in partonic and hadronic matter in the EPOS3 model with and without the hadronic afterburner UrQMD, *Phys. Rev. C* **93**, 014911 (2016).
- [57] M. Bleicher and H. Stöcker, Dynamics and freeze-out of hadron resonances at RHIC, *J. Phys. G* **30**, S111 (2004).
- [58] M. Bleicher and J. Aichelin, Strange resonance production: Probing chemical and thermal freeze-out in relativistic heavy ion collisions, *Phys. Lett. B* **530**, 81 (2002).
- [59] S. A. Bass *et al.*, Microscopic models for ultrarelativistic heavy ion collisions, *Prog. Part. Nucl. Phys.* **41**, 255 (1998).
- [60] G. Torrieri and J. Rafelski, Strange hadron resonances as a signature of freeze-out dynamics, *Phys. Lett. B* **509**, 239 (2001).
- [61] S. Acharya *et al.* (ALICE Collaboration), ALICE upgrades during the LHC long shutdown 2, *J. Instrum.* **19**, P05062 (2024).
- [62] G. Aarts, C. Allton, D. De Boni, S. Hands, B. Jäger, C. Praki, and J.-I. Skullerud, Light baryons below and above the deconfinement transition: Medium effects and parity doubling, *J. High Energy Phys.* **06** (2017) 034.
- [63] S. Acharya *et al.* (ALICE Collaboration), The ALICE experiment: A journey through QCD, *Eur. Phys. J. C* **84**, 813 (2024).
- [64] G. Aarts, C. Allton, D. De Boni, and B. Jäger, Hyperons in thermal QCD: A lattice view, *Phys. Rev. D* **99**, 074503 (2019).
- [65] C. Sasaki, Parity doubling of baryons in a chiral approach with three flavors, *Nucl. Phys.* **A970**, 388 (2018).
- [66] C. A. Dominguez, M. Loewe, and Y. Zhang, Chiral symmetry restoration and deconfinement in QCD at finite temperature, *Phys. Rev. D* **86**, 034030 (2012); **90**, 039903(E) (2014).
- [67] J. Adam *et al.* (ALICE Collaboration), Pseudorapidity and transverse-momentum distributions of charged particles in proton-proton collisions at $\sqrt{s} = 13$ TeV, *Phys. Lett. B* **753**, 319 (2016).
- [68] J. Adam *et al.* (ALICE Collaboration), Centrality dependence of the charged-particle multiplicity density at mid-rapidity in Pb-Pb collisions at $\sqrt{s_{NN}} = 5.02$ TeV, *Phys. Rev. Lett.* **116**, 222302 (2016).
- [69] S. Navas *et al.* (Particle Data Group), Review of particle physics, *Phys. Rev. D* **110**, 030001 (2024).
- [70] K. Aamodt *et al.* (ALICE Collaboration), The ALICE experiment at the CERN LHC, *J. Instrum.* **3**, S08002 (2008).
- [71] B. Abelev *et al.* (ALICE Collaboration), Performance of the ALICE experiment at the CERN LHC, *Int. J. Mod. Phys. A* **29**, 1430044 (2014).
- [72] E. Abbas *et al.* (ALICE Collaboration), Performance of the ALICE VZERO system, *J. Instrum.* **8**, P10016 (2013).
- [73] K. Aamodt *et al.* (ALICE Collaboration), Alignment of the ALICE inner tracking system with cosmic-ray tracks, *J. Instrum.* **5**, P03003 (2010).
- [74] J. Alme *et al.*, The ALICE TPC, a large 3-dimensional tracking device with fastreadout for ultra-high multiplicity events, *Nucl. Instrum. Methods Phys. Res., Sect. A* **622**, 316 (2010).
- [75] A. Akindinov *et al.*, Performance of the ALICE Time-of-Flight detector at the LHC, *Eur. Phys. J. Plus* **128**, 44 (2013).
- [76] J. Adam *et al.* (ALICE Collaboration), ALICE luminosity determination for pp collisions at $\sqrt{s} = 13$ TeV, CERN Report No. ALICE-PUBLIC-2016-002, 2016, <http://cds.cern.ch/record/2160174>.
- [77] S. Acharya *et al.* (ALICE Collaboration), Dielectron and heavy-quark production in inelastic and high-multiplicity proton-proton collisions at $\sqrt{s} = 13$ TeV, *Phys. Lett. B* **788**, 505 (2019).
- [78] S. Acharya *et al.* (ALICE Collaboration), Pseudorapidity distributions of charged particles as a function of mid- and forward rapidity multiplicities in pp collisions at $\sqrt{s} = 5.02$, 7 and 13 TeV, *Eur. Phys. J. C* **81**, 630 (2021).

- [79] S. Acharya *et al.* (ALICE Collaboration), Multiplicity dependence of (multi-)strange hadron production in proton-proton collisions at $\sqrt{s} = 13$ TeV, *Eur. Phys. J. C* **80**, 167 (2020).
- [80] K. Aamodt *et al.* (ALICE Collaboration), Strange particle production in proton-proton collisions at $\sqrt{s} = 0.9$ TeV with ALICE at the LHC, *Eur. Phys. J. C* **71**, 1594 (2011).
- [81] S. Acharya *et al.* (ALICE Collaboration), Production of light-flavor hadrons in pp collisions at $\sqrt{s} = 7$ and $\sqrt{s} = 13$ TeV, *Eur. Phys. J. C* **81**, 256 (2021).
- [82] S. Acharya *et al.* (ALICE Collaboration), Multiplicity dependence of $K^*(892)^0$ and $\Phi(1020)$ production in pp collisions at $\sqrt{s} = 13$ TeV, *Phys. Lett. B* **807**, 135501 (2020).
- [83] C. Tsallis, Possible generalization of Boltzmann-Gibbs statistics, *J. Stat. Phys.* **52**, 479 (1988).
- [84] G. Wilk and Z. Włodarczyk, Interpretation of the nonextensivity parameter q in some applications of Tsallis statistics and Lévy distributions, *Phys. Rev. Lett.* **84**, 2770 (2000).
- [85] B. I. Abelev *et al.* (STAR Collaboration), Strange particle production in $p + p$ collisions at $\sqrt{s} = 200$ GeV, *Phys. Rev. C* **75**, 064901 (2007).
- [86] T. Sjöstrand, S. Ask, J. R. Christiansen, R. Corke, N. Desai, P. Ilten, S. Mrenna, S. Prestel, C. O. Rasmussen, and P. Z. Skands, An introduction to PYTHIA 8.2, *Comput. Phys. Commun.* **191**, 159 (2015).
- [87] P. Skands, S. Carrazza, and J. Rojo, Tuning PYTHIA 8.1: The Monash 2013 Tune, *Eur. Phys. J. C* **74**, 3024 (2014).
- [88] S. Agostinelli *et al.* (GEANT4 Collaboration), GEANT4—a simulation toolkit, *Nucl. Instrum. Methods Phys. Res., Sect. A* **506**, 250 (2003).
- [89] J. Adam *et al.* (ALICE Collaboration), Multi-strange baryon production in p -Pb collisions at $\sqrt{s_{NN}} = 5.02$ TeV, *Phys. Lett. B* **758**, 389 (2016).
- [90] B. Abelev *et al.* (ALICE Collaboration), Multiplicity dependence of pion, kaon, proton and lambda production in p -Pb collisions at $\sqrt{s_{NN}} = 5.02$ TeV, *Phys. Lett. B* **728**, 25 (2014).
- [91] S. Chatterjee, A. K. Dash, and B. Mohanty, Contrasting freezeouts in large versus small systems, *J. Phys. G* **44**, 105106 (2017).
- [92] N. Sharma, J. Cleymans, B. Hippolyte, and M. Paradza, A comparison of p - p , p -Pb, Pb-Pb collisions in the thermal model: Multiplicity dependence of thermal parameters, *Phys. Rev. C* **99**, 044914 (2019).
- [93] V. Vovchenko, B. Dönigus, and H. Stoecker, Canonical statistical model analysis of p - p , p -Pb, and Pb-Pb collisions at energies available at the CERN Large Hadron Collider, *Phys. Rev. C* **100**, 054906 (2019).
- [94] F. A. Flor, G. Olinger, and R. Bellwied, System size and flavour dependence of chemical freeze-out temperatures in ALICE data from pp, pPb and PbPb collisions at LHC energies, *Phys. Lett. B* **834**, 137473 (2022).
- [95] J. Cleymans, P. M. Lo, K. Redlich, and N. Sharma, Multiplicity dependence of (multi)strange baryons in the canonical ensemble with phase shift corrections, *Phys. Rev. C* **103**, 014904 (2021).
- [96] V. Vovchenko and H. Stoecker, Thermal-FIST: A package for heavy-ion collisions and hadronic equation of state, *Comput. Phys. Commun.* **244**, 295 (2019).
- [97] S. Acharya *et al.* (ALICE Collaboration), Multiplicity-dependent production of $\Sigma(1385)^+$ and $\Xi(1530)^0$ in pp collisions at $\sqrt{s} = 13$ TeV, *J. High Energy Phys.* **05** (2024) 317.
- [98] This manuscript has associated data in a HEPData repository at: <https://www.hepdata.net/record/ins2895566>.

S. Acharya⁵⁰, A. Agarwal¹³³, G. Aglieri Rinella³², L. Aglietta^{24a,24b}, M. Agnello²⁹, N. Agrawal^{25a,25b}, Z. Ahammed¹³³, S. Ahmad¹⁵, S. U. Ahn⁷¹, I. Ahuja³⁶, A. Akindinov¹³⁹, V. Akishina³⁸, M. Al-Turany⁹⁶, D. Aleksandrov¹³⁹, B. Alessandro⁵⁶, H. M. Alfanda⁶, R. Alfaro Molina⁶⁷, B. Ali¹⁵, A. Alici^{25a,25b}, N. Alizadehvandchali¹¹⁴, A. Alkin¹⁰³, J. Alme²⁰, G. Alocco^{24a,24b}, T. Alt⁶⁴, A. R. Altamura⁵⁰, I. Altsybeev⁹⁴, J. R. Alvarado⁴⁴, M. N. Anaam⁶, C. Andrei⁴⁵, N. Andreou¹¹³, A. Andronic¹²⁴, E. Andronov¹³⁹, V. Anguelov⁹³, F. Antinori⁵⁴, P. Antonioli⁵¹, N. Apadula⁷³, L. Aphecetche¹⁰², H. Appelshäuser⁶⁴, C. Arata⁷², S. Arcelli^{25a,25b}, R. Arnaldi⁵⁶, J. G. M. C. A. Arneiro¹⁰⁹, I. C. Arsene¹⁹, M. Arslanok¹³⁶, A. Augustinus³², R. Averbek⁹⁶, D. Averyanov¹³⁹, M. D. Azmi¹⁵, H. Baba¹²², A. Badalà⁵³, J. Bae¹⁰³, Y. Bae¹⁰³, Y. W. Baek⁴⁰, X. Bai¹¹⁸, R. Bailhache⁶⁴, Y. Bailung⁴⁸, R. Bala⁹⁰, A. Baldisseri¹²⁸, B. Balis², Z. Banoo⁹⁰, V. Barbasova³⁶, F. Barile^{31a,31b}, L. Barioglio⁵⁶, M. Barlou⁷⁷, B. Barman⁴¹, G. G. Barnaföldi⁴⁶, L. S. Barnby¹¹³, E. Barreau¹⁰², V. Barret¹²⁵, L. Barreto¹⁰⁹, C. Bartels¹¹⁷, K. Barth³², E. Bartsch⁶⁴, N. Bastid¹²⁵, S. Basu⁷⁴, G. Batigne¹⁰², D. Battistini⁹⁴, B. Batyunya¹⁴⁰, D. Bauri⁴⁷, J. L. Bazo Alba¹⁰⁰, I. G. Bearden⁸², P. Becht⁹⁶, D. Behera⁴⁸, I. Belikov¹²⁷, A. D. C. Bell Hechavarria¹²⁴, F. Bellini^{25a,25b}, R. Bellwied¹¹⁴, S. Belokurova¹³⁹, L. G. E. Beltran¹⁰⁸, Y. A. V. Beltran⁴⁴, G. Bencedi⁴⁶, A. Bensaoula¹¹⁴, S. Beole^{24a,24b}, Y. Berdnikov¹³⁹, A. Berdnikova⁹³, L. Bergmann⁹³, L. Bernardinis^{23a,23b}, M. G. Besoiu⁶³, L. Betev³², P. P. Bhaduri¹³³, A. Bhasin⁹⁰, B. Bhattacharjee⁴¹, S. Bhattarai¹¹⁶, L. Bianchi^{24a,24b}, J. Bielčík³⁴, J. Bielčíková⁸⁵, A. P. Bigot¹²⁷, A. Bilandzic⁹⁴, A. Binoy¹¹⁶, G. Biro⁴⁶, S. Biswas^{4a,4b}, N. Bize¹⁰², J. T. Blair¹⁰⁷, D. Blau¹³⁹, M. B. Blidaru⁹⁶, N. Bluhme³⁸, C. Blume⁶⁴, F. Bock⁸⁶, T. Bodova²⁰, J. Bok¹⁶, L. Boldizsár⁴⁶, M. Bombara³⁶, P. M. Bond³², G. Bonomi^{55,132}, H. Borel¹²⁸, A. Borissov¹³⁹, A. G. Borquez Carcamo⁹³, E. Botta^{24a,24b}, Y. E. M. Bouziani⁶⁴, D. C. Brandibur⁶³

- L. Bratrud⁶⁴, P. Braun-Munzinger⁹⁶, M. Bregant¹⁰⁹, M. Broz³⁴, G. E. Bruno^{31a,31b,95}, V. D. Buchakchiev³⁵,
M. D. Buckland⁸⁴, D. Budnikov¹³⁹, H. Buesching⁶⁴, S. Bufalino²⁹, P. Buhler¹⁰¹, N. Burmasov¹³⁹,
Z. Buthelezi^{68,121}, A. Bylinkin²⁰, S. A. Bysiak¹⁰⁶, J. C. Cabanillas Noris¹⁰⁸, M. F. T. Cabrera¹¹⁴, H. Caines¹³⁶,
A. Caliva^{28a,28b}, E. Calvo Villar¹⁰⁰, J. M. M. Camacho¹⁰⁸, P. Camerini^{23a,23b}, F. D. M. Canedo¹⁰⁹, S. Cannito^{23a,23b},
S. L. Cantway¹³⁶, M. Carabas¹¹², A. A. Carballo³², F. Carnesecchi³², L. A. D. Carvalho¹⁰⁹,
J. Castillo Castellanos¹²⁸, M. Castoldi³², F. Catalano³², S. Cattaruzzi^{23a,23b}, R. Cerri^{24a,24b}, I. Chakaberia⁷³,
P. Chakraborty¹³⁴, S. Chandra¹³³, S. Chapeland³², M. Chartier¹¹⁷, S. Chattopadhyay¹³³, M. Chen³⁹, T. Cheng⁶,
C. Cheshkov¹²⁶, D. Chiappara^{27a,27b}, V. Chibante Barroso³², D. D. Chinellato¹⁰¹, F. Chinu^{24a,24b},
E. S. Chizzali^{94,‡}, J. Cho⁵⁸, S. Cho⁵⁸, P. Chochula³², Z. A. Chochulska¹³⁴, D. Choudhury⁴¹, S. Choudhury⁹⁸,
P. Christakoglou⁸³, C. H. Christensen⁸², P. Christiansen⁷⁴, T. Chujo¹²³, M. Ciaccio²⁹, C. Cicalo⁵²,
G. Cimador^{24a,24b}, F. Cindolo⁵¹, M. R. Ciupek⁹⁶, G. Clai^{51,§}, F. Colamaria⁵⁰, J. S. Colburn⁹⁹, D. Colella^{31a,31b},
A. Colelli^{31a,31b}, M. Colocci^{25a,25b}, M. Concas³², G. Conesa Balbastre⁷², Z. Conesa del Valle¹²⁹, G. Contin^{23a,23b},
J. G. Contreras³⁴, M. L. Coquet¹⁰², P. Cortese^{56,131}, M. R. Cosentino¹¹¹, F. Costa³², S. Costanza²¹, P. Crochet¹²⁵,
M. M. Czarnynoga¹³⁴, A. Dainese⁵⁴, G. Dange³⁸, M. C. Danisch⁹³, A. Danu⁶³, P. Das^{32,79}, S. Das^{4a,4b},
A. R. Dash¹²⁴, S. Dash⁴⁷, A. De Caro^{28a,28b}, G. de Cataldo⁵⁰, J. de Cuveland³⁸, A. De Falco^{22a,22b},
D. De Gruttola^{28a,28b}, N. De Marco⁵⁶, C. De Martin^{23a,23b}, S. De Pasquale^{28a,28b}, R. Deb¹³², R. Del Grande⁹⁴,
L. Dello Stritto³², K. C. Devereaux¹⁸, G. G. A. de Souza¹⁰⁹, P. Dhankher¹⁸, D. Di Bari^{31a,31b}, M. Di Costanzo²⁹,
A. Di Mauro³², B. Di Ruzza¹³⁰, B. Diab¹²⁸, R. A. Diaz^{7,140}, Y. Ding⁶, J. Ditzel⁶⁴, R. Divià³², Ø. Djuvsland²⁰,
U. Dmitrieva¹³⁹, A. Dobrin⁶³, B. Dönigus⁶⁴, J. M. Dubinski¹³⁴, A. Dubla⁹⁶, P. Dupieux¹²⁵, N. Dzalaiova¹³,
T. M. Eder¹²⁴, R. J. Ehlers⁷³, F. Eisenhut⁶⁴, R. Ejima⁹¹, D. Elia⁵⁰, B. Erasmus¹⁰², F. Ercolessi^{25a,25b},
B. Espagnon¹²⁹, G. Eulisse³², D. Evans⁹⁹, S. Evdokimov¹³⁹, L. Fabbietti⁹⁴, M. Faggin^{23a,23b}, J. Faivre⁷²,
F. Fan⁶, W. Fan⁷³, A. Fantoni⁴⁹, M. Fasel⁸⁶, G. Feofilov¹³⁹, A. Fernández Téllez⁴⁴, L. Ferrandi¹⁰⁹,
M. B. Ferrer³², A. Ferrero¹²⁸, C. Ferrero^{56,||}, A. Ferretti^{24a,24b}, V. J. G. Feuillard⁹³, V. Filova³⁴, D. Finogeev¹³⁹,
F. M. Fionda⁵², E. Flatland³², F. Flor¹³⁶, A. N. Flores¹⁰⁷, S. Foertsch⁶⁸, I. Fokin⁹³, S. Fokin¹³⁹, U. Follo^{56,||},
E. Fragiaco⁵⁷, E. Frajna⁴⁶, U. Fuchs³², N. Funicello^{28a,28b}, C. Furget⁷², A. Furs¹³⁹, T. Fusayasu⁹⁷,
J. J. Gaardhøje⁸², M. Gagliardi^{24a,24b}, A. M. Gago¹⁰⁰, T. Gahlaut⁴⁷, C. D. Galvan¹⁰⁸, S. Gami⁷⁹,
D. R. Gangadharan¹¹⁴, P. Ganoti⁷⁷, C. Garabatos⁹⁶, J. M. Garcia⁴⁴, T. García Chávez⁴⁴, E. Garcia-Solis⁹,
S. Garetti¹²⁹, C. Gargiulo³², P. Gasik⁹⁶, H. M. Gaur³⁸, A. Gautam¹¹⁶, M. B. Gay Ducati⁶⁶, M. Germain¹⁰²,
R. A. Gernhaeuser⁹⁴, C. Ghosh¹³³, M. Giacalone⁵¹, G. Gioachin²⁹, S. K. Giri¹³³, P. Giubellino^{56,96},
P. Giubilato^{27a,27b}, A. M. C. Glaenger¹²⁸, P. Glässel⁹³, E. Glimos¹²⁰, D. J. Q. Goh⁷⁵, V. Gonzalez¹³⁵, P. Gordeev¹³⁹,
M. Gorgon², K. Goswami⁴⁸, S. Gotovac³³, V. Grabski⁶⁷, L. K. Graczykowski¹³⁴, E. Grecka⁸⁵, A. Grelli⁵⁹,
C. Grigoras³², V. Grigoriev¹³⁹, S. Grigoryan^{1,140}, F. Grosa³², J. F. Grosse-Oetringhaus³², R. Grosso⁹⁶,
D. Grund³⁴, N. A. Grunwald⁹³, R. Guernane⁷², M. Guilbaud¹⁰², K. Gulbrandsen⁸², J. K. Gumprecht¹⁰¹,
T. Gündem⁶⁴, T. Gunji¹²², J. Guo¹⁰, W. Guo⁶, A. Gupta⁹⁰, R. Gupta⁹⁰, R. Gupta⁴⁸, K. Gwizdziel¹³⁴,
L. Gyulai⁴⁶, C. Hadjidakis¹²⁹, F. U. Haider⁹⁰, S. Haidlova³⁴, M. Haldar^{4a,4b}, H. Hamagaki⁷⁵, Y. Han¹³⁸,
B. G. Hanley¹³⁵, R. Hannigan¹⁰⁷, J. Hansen⁷⁴, M. R. Haque⁹⁶, J. W. Harris¹³⁶, A. Harton⁹, M. V. Hartung⁶⁴,
H. Hassan¹¹⁵, D. Hatzifotiadou⁵¹, P. Hauer⁴², L. B. Havener¹³⁶, E. Hellbär³², H. Helstrup³⁷, M. Hemmer⁶⁴,
T. Herman³⁴, S. G. Hernandez¹¹⁴, G. Herrera Corral⁸, S. Herrmann¹²⁶, K. F. Hetland³⁷, B. Heybeck⁶⁴,
H. Hillemanns³², B. Hippolyte¹²⁷, I. P. M. Hobus⁸³, F. W. Hoffmann⁷⁰, B. Hofman⁵⁹, M. Horst⁹⁴, A. Horzyk²,
Y. Hou⁶, P. Hristov³², P. Huhn⁶⁴, L. M. Huhta¹¹⁵, T. J. Humanic⁸⁷, A. Hutson¹¹⁴, D. Hutter³⁸, M. C. Hwang¹⁸,
R. Ilkaev¹³⁹, M. Inaba¹²³, G. M. Innocenti³², M. Ippolitov¹³⁹, A. Isakov⁸³, T. Isidori¹¹⁶, M. S. Islam^{47,98},
S. Iurchenko¹³⁹, M. Ivanov¹³, M. Ivanov⁹⁶, V. Ivanov¹³⁹, K. E. Iversen⁷⁴, M. Jablonski², B. Jacak^{18,73},
N. Jacazio^{25a,25b}, P. M. Jacobs⁷³, S. Jadlovská¹⁰⁵, J. Jadlovsky¹⁰⁵, S. Jaelani⁸¹, C. Jahnke¹¹⁰, M. J. Jakubowska¹³⁴,
M. A. Janik¹³⁴, T. Janson⁷⁰, S. Ji¹⁶, S. Jia¹⁰, T. Jiang¹⁰, A. A. P. Jimenez⁶⁵, F. Jonas⁷³, D. M. Jones¹¹⁷,
J. M. Jowett^{32,96}, J. Jung⁶⁴, M. Jung⁶⁴, A. Junique³², A. Jusko⁹⁹, J. Kaewjai¹⁰⁴, P. Kalinak⁶⁰, A. Kalweit³²,
A. Karasu Uysal¹³⁷, D. Karatovic⁸⁸, N. Karatzenis⁹⁹, O. Karavichev¹³⁹, T. Karavicheva¹³⁹, E. Karpechev¹³⁹,
M. J. Karwowska¹³⁴, U. Kebschull⁷⁰, M. Keil³², B. Ketzer⁴², J. Keul⁶⁴, S. S. Khade⁴⁸, A. M. Khan¹¹⁸,
S. Khan¹⁵, A. Khanzadeev¹³⁹, Y. Kharlov¹³⁹, A. Khatun¹¹⁶, A. Khuntia³⁴, Z. Khuranova⁶⁴, B. Kileng³⁷,
B. Kim¹⁰³, C. Kim¹⁶, D. J. Kim¹¹⁵, D. Kim¹⁰³, E. J. Kim⁶⁹, J. Kim¹³⁸, J. Kim⁵⁸, J. Kim^{32,69}, M. Kim¹⁸

S. Kim¹⁷, T. Kim¹³⁸, K. Kimura⁹¹, S. Kirsch⁶⁴, I. Kisel³⁸, S. Kiselev¹³⁹, A. Kisiel¹³⁴, J. L. Klay⁵, J. Klein³², S. Klein⁷³, C. Klein-Bösing¹²⁴, M. Kleiner⁶⁴, T. Klemenž⁹⁴, A. Kluge³², A. G. Knospe^{114,†}, C. Kobdaj¹⁰⁴, R. Kohara¹²², T. Kollegger⁹⁶, A. Kondratyev¹⁴⁰, N. Kondratyeva¹³⁹, J. König⁶⁴, S. A. Königstorfer⁹⁴, P. J. Konopka³², G. Kornakov¹³⁴, M. Korwieser⁹⁴, S. D. Koryciak², C. Koster⁸³, A. Kotliarov⁸⁵, N. Kovacic⁸⁸, V. Kovalenko¹³⁹, M. Kowalski¹⁰⁶, V. Kozuharov³⁵, G. Kozlov³⁸, I. Králik⁶⁰, A. Kravčáková³⁶, L. Krcal³², M. Krivda^{60,99}, F. Krizek⁸⁵, K. Krizkova Gajdosova³⁴, C. Krug⁶⁶, M. Krüger⁶⁴, D. M. Krupova³⁴, E. Kryshen¹³⁹, V. Kučera⁵⁸, C. Kuhn¹²⁷, P. G. Kuijper^{83,†}, T. Kumaoka¹²³, D. Kumar¹³³, L. Kumar⁸⁹, N. Kumar⁸⁹, S. Kumar⁵⁰, S. Kundu³², M. Kuo¹²³, P. Kurashvili⁷⁸, A. B. Kurepin¹³⁹, A. Kuryakin¹³⁹, S. Kushpil⁸⁵, V. Kuskov¹³⁹, M. Kutyla¹³⁴, A. Kuznetsov¹⁴⁰, M. J. Kweon⁵⁸, Y. Kwon¹³⁸, S. L. La Pointe³⁸, P. La Rocca^{26a,26b}, A. Lakrathok¹⁰⁴, M. Lamanna³², S. Lambert¹⁰², A. R. Landou⁷², R. Langoy¹¹⁹, P. Larionov³², E. Laudi³², L. Lautner⁹⁴, R. A. N. Laveaga¹⁰⁸, R. Lavicka¹⁰¹, R. Lea^{55,132}, H. Lee¹⁰³, I. Legrand⁴⁵, G. Legras¹²⁴, J. Lehrbach³⁸, A. M. Lejeune³⁴, T. M. Lelek², R. C. Lemmon^{84,†}, I. León Monzón¹⁰⁸, M. M. Lesch⁹⁴, P. Lévai⁴⁶, M. Li⁶, P. Li¹⁰, X. Li¹⁰, B. E. Liang-Gilman¹⁸, J. Lien¹¹⁹, R. Lietava⁹⁹, I. Likmeta¹¹⁴, B. Lim^{24a,24b}, H. Lim¹⁶, S. H. Lim¹⁶, S. Lin¹⁰, V. Lindenstruth³⁸, C. Lippmann⁹⁶, D. Liskova¹⁰⁵, D. H. Liu⁶, J. Liu¹¹⁷, G. S. S. Liveraro¹¹⁰, I. M. Lofnes²⁰, C. Loizides⁸⁶, S. Lokos¹⁰⁶, J. Lömker⁵⁹, X. Lopez¹²⁵, E. López Torres⁷, C. Lotteau¹²⁶, P. Lu^{96,118}, Z. Lu¹⁰, F. V. Lugo⁶⁷, J. R. Luhder¹²⁴, J. Luo³⁹, G. Luparello⁵⁷, Y. G. Ma³⁹, M. Mager³², A. Maire¹²⁷, E. M. Majerz², M. V. Makariev³⁵, M. Malaev¹³⁹, G. Malfattore^{25a,25b,51}, N. M. Malik⁹⁰, S. K. Malik⁹⁰, D. Mallick¹²⁹, N. Mallick^{48,115}, G. Mandaglio^{30,53}, S. K. Mandal⁷⁸, A. Manea⁶³, V. Manko¹³⁹, A. K. Manna⁴⁸, F. Manso¹²⁵, G. Mantzaridis⁹⁴, V. Manzari⁵⁰, Y. Mao⁶, R. W. Marcjan², G. V. Margagliotti^{23a,23b}, A. Margotti⁵¹, A. Marín⁹⁶, C. Markert¹⁰⁷, P. Martinengo³², M. I. Martínez⁴⁴, G. Martínez García¹⁰², M. P. P. Martins^{32,109}, S. Masciocchi⁹⁶, M. Maserà^{24a,24b}, A. Masoni⁵², L. Massacrier¹²⁹, O. Massen⁵⁹, A. Mastroserio^{50,130}, L. Mattei^{24a,24b,125}, S. Mattiazzo^{27a,27b}, A. Matyja¹⁰⁶, F. Mazzaschi^{24a,24b,32}, M. Mazzilli¹¹⁴, Y. Melikyan⁴³, M. Melo¹⁰⁹, A. Menchaca-Rocha⁶⁷, J. E. M. Mendez⁶⁵, E. Meninno¹⁰¹, A. S. Menon¹¹⁴, M. W. Menzel^{32,93}, M. Meres¹³, L. Micheletti³², D. Mihai¹¹², D. L. Mihaylov⁹⁴, A. U. Mikalsen²⁰, K. Mikhaylov^{139,140}, N. Minafra¹¹⁶, D. Miśkowiec⁹⁶, A. Modak^{57,132}, B. Mohanty⁷⁹, M. Mohisin Khan^{15,**}, M. A. Molander⁴³, M. M. Mondal⁷⁹, S. Monira¹³⁴, C. Mordasini¹¹⁵, D. A. Moreira De Godoy¹²⁴, I. Morozov¹³⁹, A. Morsch³², T. Mrnjavac³², V. Muccifora⁴⁹, S. Muhuri¹³³, A. Mulliri^{22a,22b}, M. G. Munhoz¹⁰⁹, R. H. Munzer⁶⁴, H. Murakami¹²², L. Musa³², J. Musinsky⁶⁰, J. W. Myrcha¹³⁴, B. Naik¹²¹, A. I. Nambrath¹⁸, B. K. Nandi⁴⁷, R. Nania⁵¹, E. Nappi⁵⁰, A. F. Nassirpour¹⁷, V. Nastase¹¹², A. Nath⁹³, N. F. Nathanson⁸², C. Natrass¹²⁰, K. Naumov¹⁸, M. N. Naydenov³⁵, A. Neagu¹⁹, A. Negru¹¹², L. Nellen⁶⁵, R. Nepeivoda⁷⁴, S. Nese¹⁹, N. Nicassio^{31a,31b}, B. S. Nielsen⁸², E. G. Nielsen⁸², S. Nikolaev¹³⁹, V. Nikulin¹³⁹, F. Noferini⁵¹, S. Noh¹², P. Nomokonov¹⁴⁰, J. Norman¹¹⁷, N. Novitzky⁸⁶, A. Nyanin¹³⁹, J. Nystrand²⁰, M. R. Ockleton¹¹⁷, M. Ogino⁷⁵, S. Oh¹⁷, A. Ohlson⁷⁴, V. A. Okorokov¹³⁹, J. Oleniacz¹³⁴, A. Onnerstad¹¹⁵, C. Oppedisano⁵⁶, A. Ortiz Velasquez⁶⁵, J. Otwinowski¹⁰⁶, M. Oya⁹¹, K. Oyama⁷⁵, S. Padhan⁴⁷, D. Pagano^{55,132}, G. Paic⁶⁵, S. Paisano-Guzmán⁴⁴, A. Palasciano⁵⁰, I. Panasenko⁷⁴, S. Panebianco¹²⁸, P. Panigrahi⁴⁷, C. Pantouvakis^{27a,27b}, H. Park¹²³, J. Park¹²³, S. Park¹⁰³, J. E. Parkkila³², Y. Patley⁴⁷, R. N. Patra⁵⁰, P. Paudel¹¹⁶, B. Paul¹³³, H. Pei⁶, T. Peitzmann⁵⁹, X. Peng¹¹, M. Pennisi^{24a,24b}, S. Perciballi^{24a,24b}, D. Peresunko¹³⁹, G. M. Perez⁷, Y. Pestov¹³⁹, M. T. Petersen⁸², V. Petrov¹³⁹, M. Petrovici⁴⁵, S. Piano⁵⁷, M. Pikna¹³, P. Pillot¹⁰², O. Pinazza^{32,51}, L. Pinsky¹¹⁴, C. Pinto⁹⁴, S. Pisano⁴⁹, M. Płoskoń⁷³, M. Planinic⁸⁸, D. K. Plociennik², M. G. Poghosyan⁸⁶, B. Polichtchouk¹³⁹, S. Politano²⁹, N. Poljak⁸⁸, A. Pop⁴⁵, S. Porteboeuf-Houssais¹²⁵, V. Pozdniakov^{140,†}, I. Y. Pozos⁴⁴, K. K. Pradhan⁴⁸, S. K. Prasad^{4a,4b}, S. Prasad⁴⁸, R. Preghenella⁵¹, F. Prino⁵⁶, C. A. Pruneau¹³⁵, I. Pshenichnov¹³⁹, M. Puccio³², S. Pucillo^{24a,24b}, S. Qiu⁸³, L. Quaglia^{24a,24b}, A. M. K. Radhakrishnan⁴⁸, S. Ragoni¹⁴, A. Rai¹³⁶, A. Rakotozafindrabe¹²⁸, L. Ramello^{56,131}, C. O. Ramirez-Alvarez⁴⁴, M. Rasa^{26a,26b}, S. S. Räsänen⁴³, R. Rath⁵¹, M. P. Rauch²⁰, I. Ravasenga³², K. F. Read^{86,120}, C. Reckziegel¹¹¹, A. R. Redelbach³⁸, K. Redlich^{78,††}, C. A. Reetz⁹⁶, H. D. Regules-Medel⁴⁴, A. Rehman²⁰, F. Reidt³², H. A. Reme-Ness³⁷, K. Reygers⁹³, A. Riabov¹³⁹, V. Riabov¹³⁹, R. Ricci^{28a,28b}, M. Richter²⁰, A. A. Riedel⁹⁴, W. Riegler³², A. G. Riffero^{24a,24b}, M. Rignanese^{27a,27b}, C. Ripoli^{28a,28b}, C. Ristea⁶³, M. V. Rodriguez³², M. Rodríguez Cahuantzi⁴⁴, S. A. Rodríguez Ramírez⁴⁴, K. Røed¹⁹, R. Rogalev¹³⁹, E. Rogochaya¹⁴⁰, T. S. Rogoschinski⁶⁴, D. Rohr³², D. Röhrich²⁰, S. Rojas Torres³⁴, P. S. Rokita¹³⁴, G. Romanenko^{25a,25b}

F. Ronchetti³², D. Rosales Herrera⁴⁴, E. D. Rosas⁶⁵, K. Roslon¹³⁴, A. Rossi⁵⁴, A. Roy⁴⁸, S. Roy⁴⁷, N. Rubini⁵¹, J. A. Rudolph⁸³, D. Ruggiano¹³⁴, R. Rui^{23a,23b}, P. G. Russek², R. Russo⁸³, A. Rustamov⁸⁰, E. Ryabinkin¹³⁹, Y. Ryabov¹³⁹, A. Rybicki¹⁰⁶, L. C. V. Ryder¹¹⁶, J. Ryu¹⁶, W. Rzeska¹³⁴, B. Sabiu⁵¹, S. Sadovsky¹³⁹, J. Saetre²⁰, S. Saha⁷⁹, B. Sahoo⁴⁸, R. Sahoo⁴⁸, D. Sahu⁴⁸, P. K. Sahu⁶¹, J. Saini¹³³, K. Sajdakova³⁶, S. Sakai¹²³, M. P. Salvan⁹⁶, S. Sambyal⁹⁰, D. Samitz¹⁰¹, I. Sanna^{32,94}, T. B. Saramela¹⁰⁹, D. Sarkar⁸², P. Sarma⁴¹, V. Sarritzu^{22a,22b}, V. M. Sarti⁹⁴, M. H. P. Sas³², S. Sawan⁷⁹, E. Scapparone⁵¹, J. Schambach⁸⁶, H. S. Scheid^{32,64}, C. Schiaua⁴⁵, R. Schicker⁹³, F. Schlepfer^{32,93}, A. Schmah⁹⁶, C. Schmidt⁹⁶, M. O. Schmidt³², M. Schmidt⁹², N. V. Schmidt⁸⁶, A. R. Schmier¹²⁰, J. Schoengarth⁶⁴, R. Schotter¹⁰¹, A. Schröter³⁸, J. Schukraft³², K. Schweda⁹⁶, G. Scioli^{25a,25b}, E. Scomparin⁵⁶, J. E. Seger¹⁴, Y. Sekiguchi¹²², D. Sekihata¹²², M. Selina⁸³, I. Selyuzhenkov⁹⁶, S. Senyukov¹²⁷, J. J. Seo⁹³, D. Serebryakov¹³⁹, L. Serkin^{65,‡}, L. Šerkšnytė⁹⁴, A. Sevcenco⁶³, T. J. Shaba⁶⁸, A. Shabetai¹⁰², R. Shahoyan³², A. Shangaraev¹³⁹, B. Sharma⁹⁰, D. Sharma⁴⁷, H. Sharma⁵⁴, M. Sharma⁹⁰, S. Sharma⁹⁰, U. Sharma⁹⁰, A. Shatat¹²⁹, O. Sheibani^{114,135}, K. Shigaki⁹¹, M. Shimomura⁷⁶, S. Shirinkin¹³⁹, Q. Shou³⁹, Y. Sibiriak¹³⁹, S. Siddhanta⁵², T. Siemiarz⁷⁸, T. F. Silva¹⁰⁹, D. Silvermyr⁷⁴, T. Simantathammakul¹⁰⁴, R. Simeonov³⁵, B. Singh⁹⁰, B. Singh⁹⁴, K. Singh⁴⁸, R. Singh⁷⁹, R. Singh^{54,96}, S. Singh¹⁵, V. K. Singh¹³³, V. Singhal¹³³, T. Sinha⁹⁸, B. Sitar¹³, M. Sitta^{56,131}, T. B. Skaali¹⁹, G. Skorodumovs⁹³, N. Smirnov¹³⁶, R. J. M. Snellings⁵⁹, E. H. Solheim¹⁹, C. Sonnabend^{32,96}, J. M. Sonneveld⁸³, F. Soramel^{27a,27b}, A. B. Soto-Hernandez⁸⁷, R. Spijkers⁸³, I. Sputowska¹⁰⁶, J. Staa⁷⁴, J. Stachel⁹³, I. Stan⁶³, P. J. Steffanic¹²⁰, T. Stellhorn¹²⁴, S. F. Stiefelmaier⁹³, D. Stocco¹⁰², I. Storehaug¹⁹, N. J. Strangmann⁶⁴, P. Stratmann¹²⁴, S. Strazzi^{25a,25b}, A. Sturniolo^{30,53}, C. P. Stylianidis⁸³, A. A. P. Suaide¹⁰⁹, C. Suire¹²⁹, A. Suiu^{32,112}, M. Sukhanov¹³⁹, M. Suljic³², R. Sultanov¹³⁹, V. Sumberia⁹⁰, S. Sumowidagdo⁸¹, L. H. Tabares⁷, S. F. Taghavi⁹⁴, J. Takahashi¹¹⁰, G. J. Tambave⁷⁹, S. Tang⁶, Z. Tang¹¹⁸, J. D. Tapia Takaki¹¹⁶, N. Tapus¹¹², L. A. Tarasovicova³⁶, M. G. Tazila⁴⁵, A. Tauro³², A. Tavira García¹²⁹, G. Tejeda Muñoz⁴⁴, L. Terlizzi^{24a,24b}, C. Terrevoli⁵⁰, D. Thakur^{24a,24b}, S. Thakur^{4a,4b}, M. Thogersen¹⁹, D. Thomas¹⁰⁷, A. Tikhonov¹³⁹, N. Tiltmann^{32,124}, A. R. Timmins¹¹⁴, M. Tkacik¹⁰⁵, T. Tkacik¹⁰⁵, A. Toia⁶⁴, R. Tokumoto⁹¹, S. Tomassini^{25a,25b}, K. Tomohiro⁹¹, N. Topilskaya¹³⁹, M. Toppi⁴⁹, V. V. Torres¹⁰², A. G. Torres Ramos^{31a,31b}, A. Trifiró^{30,53}, T. Triloki⁹⁵, A. S. Triolo^{30,32,53}, S. Tripathy³², T. Tripathy^{47,125}, S. Trogolo^{24a,24b}, V. Trubnikov³, W. H. Trzaska¹¹⁵, T. P. Trzcinski¹³⁴, C. Tsolanta¹⁹, R. Tu³⁹, A. Tumkin¹³⁹, R. Turrisi⁵⁴, T. S. Tveter¹⁹, K. Ullaland²⁰, B. Ulukutlu⁹⁴, S. Upadhyaya¹⁰⁶, A. Uras¹²⁶, G. L. Usai^{22a,22b}, M. Vaid⁹⁰, M. Vala³⁶, N. Valle⁵⁵, L. V. R. van Doremalen⁵⁹, M. van Leeuwen⁸³, C. A. van Veen⁹³, R. J. G. van Weelden⁸³, P. Vande Vyvre³², D. Varga⁴⁶, Z. Varga^{46,136}, P. Vargas Torres⁶⁵, M. Vasileiou⁷⁷, A. Vasiliev^{139,†}, O. Vázquez Doce⁴⁹, O. Vazquez Rueda¹¹⁴, V. Vechernin¹³⁹, P. Veen¹²⁸, E. Vercellin^{24a,24b}, R. Verma⁴⁷, R. Vértesi⁴⁶, M. Verweij⁵⁹, L. Vickovic³³, Z. Vilakazi¹²¹, O. Villalobos Baillie⁹⁹, A. Villani^{23a,23b}, A. Vinogradov¹³⁹, T. Virgili^{28a,28b}, M. M. O. Virda¹¹⁵, A. Vodopyanov¹⁴⁰, B. Volkel³², M. A. Völkl⁹³, S. A. Voloshin¹³⁵, G. Volpe^{31a,31b}, B. von Haller³², I. Vorobyev³², N. Vozniuk¹³⁹, J. Vrláková³⁶, J. Wan³⁹, C. Wang³⁹, D. Wang³⁹, Y. Wang³⁹, Y. Wang⁶, Z. Wang³⁹, A. Wegrzynek³², F. T. Weighofer³⁸, S. C. Wenzel³², J. P. Wessels¹²⁴, P. K. Wiacek², J. Wiechula⁶⁴, J. Wikne¹⁹, G. Wilk⁷⁸, J. Wilkinson⁹⁶, G. A. Willems¹²⁴, B. Windelband⁹³, M. Winn¹²⁸, J. R. Wright¹⁰⁷, W. Wu³⁹, Y. Wu¹¹⁸, Z. Xiong¹¹⁸, R. Xu⁶, A. Yadav⁴², A. K. Yadav¹³³, Y. Yamaguchi⁹¹, S. Yang²⁰, S. Yano⁹¹, E. R. Yeats¹⁸, J. Yi⁶, Z. Yin⁶, I.-K. Yoo¹⁶, J. H. Yoon⁵⁸, H. Yu¹², S. Yuan²⁰, A. Yuncu⁹³, V. Zaccolo^{23a,23b}, C. Zampolli³², F. Zanone⁹³, N. Zardoshti³², A. Zarochentsev¹³⁹, P. Závada⁶², N. Zaviyalov¹³⁹, M. Zhalov¹³⁹, B. Zhang⁹³, C. Zhang¹²⁸, L. Zhang³⁹, M. Zhang^{6,125}, M. Zhang⁶, S. Zhang³⁹, X. Zhang⁶, Y. Zhang¹¹⁸, Y. Zhang¹¹⁸, Z. Zhang⁶, M. Zhao¹⁰, V. Zhrebchevskii¹³⁹, Y. Zhi¹⁰, D. Zhou⁶, Y. Zhou⁸², J. Zhu^{6,54}, S. Zhu^{96,118}, Y. Zhu⁶, S. C. Zugeravel⁵⁶ and N. Zurlo^{55,132}

(ALICE Collaboration)

¹*A.I. Alikhanyan National Science Laboratory (Yerevan Physics Institute) Foundation, Yerevan, Armenia*²*AGH University of Krakow, Krakow, Poland*³*Bogolyubov Institute for Theoretical Physics, National Academy of Sciences of Ukraine, Kiev, Ukraine*^{4a}*Bose Institute, Department of Physics, Kolkata, India*^{4b}*Centre for Astroparticle Physics and Space Science (CAPSS), Kolkata, India*

- ⁵California Polytechnic State University, San Luis Obispo, California, USA
- ⁶Central China Normal University, Wuhan, China
- ⁷Centro de Aplicaciones Tecnológicas y Desarrollo Nuclear (CEADEN), Havana, Cuba
- ⁸Centro de Investigación y de Estudios Avanzados (CINVESTAV), Mexico City and Mérida, Mexico
- ⁹Chicago State University, Chicago, Illinois, USA
- ¹⁰China Nuclear Data Center, China Institute of Atomic Energy, Beijing, China
- ¹¹China University of Geosciences, Wuhan, China
- ¹²Chungbuk National University, Cheongju, Republic of Korea
- ¹³Comenius University Bratislava, Faculty of Mathematics, Physics and Informatics, Bratislava, Slovak Republic
- ¹⁴Creighton University, Omaha, Nebraska, USA
- ¹⁵Department of Physics, Aligarh Muslim University, Aligarh, India
- ¹⁶Department of Physics, Pusan National University, Pusan, Republic of Korea
- ¹⁷Department of Physics, Sejong University, Seoul, Republic of Korea
- ¹⁸Department of Physics, University of California, Berkeley, California, USA
- ¹⁹Department of Physics, University of Oslo, Oslo, Norway
- ²⁰Department of Physics and Technology, University of Bergen, Bergen, Norway
- ²¹Dipartimento di Fisica, Università di Pavia, Pavia, Italy
- ^{22a}Dipartimento di Fisica dell'Università, Cagliari, Italy
- ^{22b}Sezione INFN, Cagliari, Italy
- ^{23a}Dipartimento di Fisica dell'Università, Trieste, Italy
- ^{23b}Sezione INFN, Trieste, Italy
- ^{24a}Dipartimento di Fisica dell'Università, Turin, Italy
- ^{24b}Sezione INFN, Turin, Italy
- ^{25a}Dipartimento di Fisica e Astronomia dell'Università, Bologna, Italy
- ^{25b}Sezione INFN, Bologna, Italy
- ^{26a}Dipartimento di Fisica e Astronomia dell'Università, Catania, Italy
- ^{26b}Sezione INFN, Catania, Italy
- ^{27a}Dipartimento di Fisica e Astronomia dell'Università, Padova, Italy
- ^{27b}Sezione INFN, Padova, Italy
- ^{28a}Dipartimento di Fisica 'E.R. Caianiello' dell'Università, Salerno, Italy
- ^{28b}Gruppo Collegato INFN, Salerno, Italy
- ²⁹Dipartimento DISAT del Politecnico and Sezione INFN, Turin, Italy
- ³⁰Dipartimento di Scienze MIFT, Università di Messina, Messina, Italy
- ^{31a}Dipartimento Interateneo di Fisica "M. Merlin," Bari, Italy
- ^{31b}Sezione INFN, Bari, Italy
- ³²European Organization for Nuclear Research (CERN), Geneva, Switzerland
- ³³Faculty of Electrical Engineering, Mechanical Engineering and Naval Architecture, University of Split, Split, Croatia
- ³⁴Faculty of Nuclear Sciences and Physical Engineering, Czech Technical University in Prague, Prague, Czech Republic
- ³⁵Faculty of Physics, Sofia University, Sofia, Bulgaria
- ³⁶Faculty of Science, P.J. Šafárik University, Košice, Slovak Republic
- ³⁷Faculty of Technology, Environmental and Social Sciences, Bergen, Norway
- ³⁸Frankfurt Institute for Advanced Studies, Johann Wolfgang Goethe-Universität Frankfurt, Frankfurt, Germany
- ³⁹Fudan University, Shanghai, China
- ⁴⁰Gangneung-Wonju National University, Gangneung, Republic of Korea
- ⁴¹Gauhati University, Department of Physics, Guwahati, India
- ⁴²Helmholtz-Institut für Strahlen- und Kernphysik, Rheinische Friedrich-Wilhelms-Universität Bonn, Bonn, Germany
- ⁴³Helsinki Institute of Physics (HIP), Helsinki, Finland
- ⁴⁴High Energy Physics Group, Universidad Autónoma de Puebla, Puebla, Mexico
- ⁴⁵Horia Hulubei National Institute of Physics and Nuclear Engineering, Bucharest, Romania
- ⁴⁶HUN-REN Wigner Research Centre for Physics, Budapest, Hungary
- ⁴⁷Indian Institute of Technology Bombay (IIT), Mumbai, India
- ⁴⁸Indian Institute of Technology Indore, Indore, India
- ⁴⁹INFN, Laboratori Nazionali di Frascati, Frascati, Italy
- ⁵⁰INFN, Sezione di Bari, Bari, Italy
- ⁵¹INFN, Sezione di Bologna, Bologna, Italy

- ⁵²INFN, Sezione di Cagliari, Cagliari, Italy
⁵³INFN, Sezione di Catania, Catania, Italy
⁵⁴INFN, Sezione di Padova, Padova, Italy
⁵⁵INFN, Sezione di Pavia, Pavia, Italy
⁵⁶INFN, Sezione di Torino, Turin, Italy
⁵⁷INFN, Sezione di Trieste, Trieste, Italy
⁵⁸Inha University, Incheon, Republic of Korea
⁵⁹Institute for Gravitational and Subatomic Physics (GRASP),
Utrecht University/Nikhef, Utrecht, Netherlands
⁶⁰Institute of Experimental Physics, Slovak Academy of Sciences, Košice, Slovak Republic
⁶¹Institute of Physics, Homi Bhabha National Institute, Bhubaneswar, India
⁶²Institute of Physics of the Czech Academy of Sciences, Prague, Czech Republic
⁶³Institute of Space Science (ISS), Bucharest, Romania
⁶⁴Institut für Kernphysik, Johann Wolfgang Goethe-Universität Frankfurt, Frankfurt, Germany
⁶⁵Instituto de Ciencias Nucleares, Universidad Nacional Autónoma de México, Mexico City, Mexico
⁶⁶Instituto de Física, Universidade Federal do Rio Grande do Sul (UFRGS), Porto Alegre, Brazil
⁶⁷Instituto de Física, Universidad Nacional Autónoma de México, Mexico City, Mexico
⁶⁸iThemba LABS, National Research Foundation, Somerset West, South Africa
⁶⁹Jeonbuk National University, Jeonju, Republic of Korea
⁷⁰Johann-Wolfgang-Goethe Universität Frankfurt Institut für Informatik, Fachbereich Informatik und
Mathematik, Frankfurt, Germany
⁷¹Korea Institute of Science and Technology Information, Daejeon, Republic of Korea
⁷²Laboratoire de Physique Subatomique et de Cosmologie, Université Grenoble-Alpes, CNRS-IN2P3,
Grenoble, France
⁷³Lawrence Berkeley National Laboratory, Berkeley, California, USA
⁷⁴Lund University Department of Physics, Division of Particle Physics, Lund, Sweden
⁷⁵Nagasaki Institute of Applied Science, Nagasaki, Japan
⁷⁶Nara Women's University (NWU), Nara, Japan
⁷⁷National and Kapodistrian University of Athens, School of Science, Department of Physics,
Athens, Greece
⁷⁸National Centre for Nuclear Research, Warsaw, Poland
⁷⁹National Institute of Science Education and Research, Homi Bhabha National Institute, Jatni, India
⁸⁰National Nuclear Research Center, Baku, Azerbaijan
⁸¹National Research and Innovation Agency—BRIN, Jakarta, Indonesia
⁸²Niels Bohr Institute, University of Copenhagen, Copenhagen, Denmark
⁸³Nikhef, National Institute for Subatomic Physics, Amsterdam, Netherlands
⁸⁴Nuclear Physics Group, STFC Daresbury Laboratory, Daresbury, United Kingdom
⁸⁵Nuclear Physics Institute of the Czech Academy of Sciences, Husinec-Řež, Czech Republic
⁸⁶Oak Ridge National Laboratory, Oak Ridge, Tennessee, USA
⁸⁷Ohio State University, Columbus, Ohio, USA
⁸⁸Physics department, Faculty of Science, University of Zagreb, Zagreb, Croatia
⁸⁹Physics Department, Panjab University, Chandigarh, India
⁹⁰Physics Department, University of Jammu, Jammu, India
⁹¹Physics Program and International Institute for Sustainability with Knotted Chiral Meta Matter (WPI-
SKCM²), Hiroshima University, Hiroshima, Japan
⁹²Physikalisches Institut, Eberhard-Karls-Universität Tübingen, Tübingen, Germany
⁹³Physikalisches Institut, Ruprecht-Karls-Universität Heidelberg, Heidelberg, Germany
⁹⁴Physik Department, Technische Universität München, Munich, Germany
⁹⁵Politecnico di Bari and Sezione INFN, Bari, Italy
⁹⁶Research Division and ExtreMe Matter Institute EMMI,
GSI Helmholtzzentrum für Schwerionenforschung GmbH, Darmstadt, Germany
⁹⁷Saga University, Saga, Japan
⁹⁸Saha Institute of Nuclear Physics, Homi Bhabha National Institute, Kolkata, India
⁹⁹School of Physics and Astronomy, University of Birmingham, Birmingham, United Kingdom
¹⁰⁰Sección Física, Departamento de Ciencias, Pontificia Universidad Católica del Perú, Lima, Peru
¹⁰¹Stefan Meyer Institut für Subatomare Physik (SMI), Vienna, Austria
¹⁰²SUBATECH, IMT Atlantique, Nantes Université, CNRS-IN2P3, Nantes, France
¹⁰³Sungkyunkwan University, Suwon City, Republic of Korea
¹⁰⁴Suranaree University of Technology, Nakhon Ratchasima, Thailand
¹⁰⁵Technical University of Košice, Košice, Slovak Republic

- ¹⁰⁶*The Henryk Niewodniczanski Institute of Nuclear Physics, Polish Academy of Sciences, Krakow, Poland*
- ¹⁰⁷*The University of Texas at Austin, Austin, Texas, USA*
- ¹⁰⁸*Universidad Autónoma de Sinaloa, Culiacán, Mexico*
- ¹⁰⁹*Universidade de São Paulo (USP), São Paulo, Brazil*
- ¹¹⁰*Universidade Estadual de Campinas (UNICAMP), Campinas, Brazil*
- ¹¹¹*Universidade Federal do ABC, Santo Andre, Brazil*
- ¹¹²*Universitatea Nationala de Stiinta si Tehnologie Politehnica Bucuresti, Bucharest, Romania*
- ¹¹³*University of Derby, Derby, United Kingdom*
- ¹¹⁴*University of Houston, Houston, Texas, USA*
- ¹¹⁵*University of Jyväskylä, Jyväskylä, Finland*
- ¹¹⁶*University of Kansas, Lawrence, Kansas, USA*
- ¹¹⁷*University of Liverpool, Liverpool, United Kingdom*
- ¹¹⁸*University of Science and Technology of China, Hefei, China*
- ¹¹⁹*University of South-Eastern Norway, Kongsberg, Norway*
- ¹²⁰*University of Tennessee, Knoxville, Tennessee, USA*
- ¹²¹*University of the Witwatersrand, Johannesburg, South Africa*
- ¹²²*University of Tokyo, Tokyo, Japan*
- ¹²³*University of Tsukuba, Tsukuba, Japan*
- ¹²⁴*Universität Münster, Institut für Kernphysik, Münster, Germany*
- ¹²⁵*Université Clermont Auvergne, CNRS/IN2P3, LPC, Clermont-Ferrand, France*
- ¹²⁶*Université de Lyon, CNRS/IN2P3, Institut de Physique des 2 Infinis de Lyon, Lyon, France*
- ¹²⁷*Université de Strasbourg, CNRS, IPHC UMR 7178, F-67000 Strasbourg, France, Strasbourg, France*
- ¹²⁸*Université Paris-Saclay, Centre d'Etudes de Saclay (CEA), IRFU, Département de Physique Nucléaire (DPhN), Saclay, France*
- ¹²⁹*Université Paris-Saclay, CNRS/IN2P3, IJCLab, Orsay, France*
- ¹³⁰*Università degli Studi di Foggia, Foggia, Italy*
- ¹³¹*Università del Piemonte Orientale, Vercelli, Italy*
- ¹³²*Università di Brescia, Brescia, Italy*
- ¹³³*Variable Energy Cyclotron Centre, Homi Bhabha National Institute, Kolkata, India*
- ¹³⁴*Warsaw University of Technology, Warsaw, Poland*
- ¹³⁵*Wayne State University, Detroit, Michigan, USA*
- ¹³⁶*Yale University, New Haven, Connecticut, USA*
- ¹³⁷*Yildiz Technical University, Istanbul, Turkey*
- ¹³⁸*Yonsei University, Seoul, Republic of Korea*
- ¹³⁹*Affiliated with an institute formerly covered by a cooperation agreement with CERN*
- ¹⁴⁰*Affiliated with an international laboratory covered by a cooperation agreement with CERN*

[†]Deceased.

[‡]Also at Max-Planck-Institut für Physik, Munich, Germany.

[§]Also at Italian National Agency for New Technologies, Energy and Sustainable Economic Development (ENEA), Bologna, Italy.

^{||}Also at Dipartimento DET del Politecnico di Torino, Turin, Italy.

[¶]Also at Lehigh University, USA.

^{**}Also at Department of Applied Physics, Aligarh Muslim University, Aligarh, India.

^{††}Also at Institute of Theoretical Physics, University of Wrocław, Poland.

^{‡‡}Also at Facultad de Ciencias, Universidad Nacional Autónoma de México, Mexico City, Mexico.